

A Parametric Finite Element Approach for an Anisotropic Multi-Phase Mullins–Sekerka Problem with Kinetic Undercooling

Tokuhiro Eto* Harald Garcke† Robert Nürnberg‡

Abstract

We consider a sharp interface formulation for an anisotropic multi-phase Mullins–Sekerka problem with kinetic undercooling. The flow is characterized by a cluster of surfaces evolving such that the total surface energy plus a weighted sum of the volumes of the enclosed phases decreases in time. Upon deriving a suitable variational formulation, we introduce a fully discrete unfitted finite element method. In this approach, the approximations of the moving interfaces are independent of the triangulations used for the equations in the bulk. Our method can be shown to be unconditionally stable. Several numerical examples demonstrate the capabilities of the introduced method. In particular, it is demonstrated that the evolution of multiple ice crystals with junctions can be modeled using the proposed approach.

Keywords: Mullins–Sekerka problem, multi-phase, parametric finite element method, unconditional stability, anisotropy, ice crystal growth.

AMS Subject Classification: Primary: 65M12; Secondary: 35R35, 65M50, 65M60, 74N10, 80A22.

1 Introduction

Crystal growth driven by diffusion and anisotropic surface energy leads to fascinating pattern formation phenomena in nature. In addition, the understanding of such crystallization processes is fundamental for many applications in engineering and in particular in the foundry industry and we refer to [25] for more details on phase transformations in multi-phase systems. In this paper, we consider a sharp interface model for an anisotropic multi-phase Mullins–Sekerka problem, which describes the evolution of a system that can exhibit more than two phases and is governed by a quasi-static diffusion equation. More precisely, we study the evolution of a curve network/surface cluster in a bounded Lipschitz domain Ω in \mathbb{R}^d , $d = 2, 3$. The cluster Γ is made up of several interfaces Γ_i , which can meet at triple junctions \mathcal{T}_k , and which separate the bounded domain $\Omega \subset \mathbb{R}^d$ into regions \mathcal{R}_ℓ belonging to different phases, $\ell \in \mathbb{N}_{\leq I_R} := \{1, \dots, I_R\}$, $I_R \geq 2$. The model describes the evolution of the surface cluster such that the anisotropic interfacial energy is decreased over time. The flow is principally driven by fluxes across interfaces that are derived from chemical potentials $\mathbf{w} = (w_1, \dots, w_{I_R})^\top$, which satisfy diffusion equations in the bulk. We remark, that in some applications the vector \mathbf{w} also describes concentrations of chemical substances. For example, in ice crystal growth \mathbf{w} is related to vapor number densities.

*Université Claude Bernard Lyon 1, CNRS, Centrale Lyon, INSA Lyon, Université Jean Monnet, ICJ UMR5208, 69622 Villeurbanne, France. E-mail: eto@math.univ-lyon1.fr

†Fakultät für Mathematik, Universität Regensburg, 93040 Regensburg, Germany. E-mail: harald.garcke@ur.de

‡Dipartimento di Matematica, Università di Trento, 38123 Trento, Italy. E-mail: robert.nurnberg@unitn.it

In addition, the evolving cluster satisfies an anisotropic Gibbs–Thomson law featuring effects due to kinetic undercooling. Overall, the model seeks a vector of chemical potentials $\mathbf{w} : \Omega \rightarrow \mathbb{R}^{I_R}$ and an evolving surface cluster $(\Gamma(t))_{t \in [0, T]}$ such that

$$\Delta \mathbf{w} = \mathbf{0} \quad \text{in } \Omega \setminus \Gamma(t), \quad t \in (0, T], \quad (1.1a)$$

$$[\mathbf{w}]_{\Gamma_i} = \mathbf{0} \quad \text{on } \Gamma_i(t), \quad t \in (0, T], \quad i \in \mathbb{N}_{\leq I_S}, \quad (1.1b)$$

$$\mathbf{w} \cdot [\boldsymbol{\chi}]_{\Gamma_i} = \varkappa_{\gamma, i} - \frac{V_i \rho_i}{\beta_i(\vec{\nu}_i)} \quad \text{on } \Gamma_i(t), \quad t \in (0, T], \quad i \in \mathbb{N}_{\leq I_S}, \quad (1.1c)$$

$$[\nabla \mathbf{w}]_{\Gamma_i} \cdot \vec{\nu}_i = -V_i [\boldsymbol{\chi}]_{\Gamma_i} \quad \text{on } \Gamma_i(t), \quad t \in (0, T], \quad i \in \mathbb{N}_{\leq I_S}, \quad (1.1d)$$

$$\sum_{\ell=1}^3 \left\{ \gamma_{s_\ell^k}(\vec{\nu}_{s_\ell^k}) \vec{\mu}_{s_\ell^k} - \left(\gamma'_{s_\ell^k}(\vec{\nu}_{s_\ell^k}) \cdot \vec{\mu}_{s_\ell^k} \right) \vec{\nu}_{s_\ell^k} \right\} = \vec{0} \quad \text{on } \mathcal{T}_k(t), \quad t \in (0, T], \quad k \in \mathbb{N}_{\leq I_T}, \quad (1.1e)$$

$$\nabla_{\vec{\nu}_\Omega} \mathbf{w} = O \quad \text{on } \partial\Omega_N, \quad (1.1f)$$

$$\mathbf{w} = \mathbf{w}_D \quad \text{on } \partial\Omega_D, \quad (1.1g)$$

$$\Gamma(0) = \Gamma_0, \quad (1.1h)$$

where $T > 0$ is a final time. Here $\vec{\nu}_i$, V_i and $\varkappa_{\gamma, i}$ denote a unit normal, the associated normal velocity and the anisotropic mean curvature of the surfaces making up the cluster $\Gamma(t) = \bigcup_{i=1}^{I_S} \Gamma_i(t)$, with $I_S \geq 1$. For a quantity q , we define the jump of q across $\Gamma_i(t)$ in the direction of the unit normal $\vec{\nu}_i$ by $[q]_{\Gamma_i} := \lim_{\varepsilon \downarrow 0} \{q(\cdot + \varepsilon \vec{\nu}_i) - q(\cdot - \varepsilon \vec{\nu}_i)\}$. Moreover, $\rho_i \geq 0$ are kinetic coefficients and $\beta_i : \mathbb{S}^{d-1} \rightarrow \mathbb{R}_{>0}$ describe orientation-dependent mobility functions which are assumed to be smooth, even and positive functions defined on the unit sphere. In addition, $\boldsymbol{\chi} = (\chi_1, \dots, \chi_{I_R})^\top$ denotes the vector of the characteristic functions χ_ℓ of the regions \mathcal{R}_ℓ . Hence (1.1c) describes an anisotropic Gibbs–Thomson law with kinetic undercooling. The equation (1.1d) describes an interfacial mass balance, see [14, 21]. On triple junctions the force balance condition (1.1e) must hold, which involves the normals and conormals of the three surfaces meeting at a junction \mathcal{T}_k . For a geometric and physical interpretation of this force balance condition we refer to [26, 22] and [8, p. 199]. The precise definitions and formulations will be stated in Section 2. To close the system, we impose the boundary conditions (1.1f), (1.1g) and the initial condition (1.1h). For the former two, we have split the boundary $\partial\Omega$, with outer normal $\vec{\nu}_\Omega$ into the relatively open subsets $\partial\Omega_D$ and $\partial\Omega_N$, such that $\partial\Omega = \partial\Omega_D \cup \partial\Omega_N$ and $\partial\Omega_D \cap \partial\Omega_N = \emptyset$, for the Dirichlet and Neumann boundary conditions that are imposed on the chemical potential, respectively. By $\nabla_{\vec{\nu}_\Omega}$ we denote the spatial derivative in the direction of the normal $\vec{\nu}_\Omega$. With the help of the Dirichlet data \mathbf{w}_D , we can model undercooling and supersaturation at an outer boundary, see, e.g. [9] for the two-phase case. Throughout this work, we assume for simplicity that \mathbf{w}_D is constant. The model (1.1) is an anisotropic version of the model studied in [12, 18] which also takes kinetic undercooling into account. For the modifications needed to include anisotropy, we refer to [22] and for a discussion how to model kinetic undercooling, we refer to [14].

Other approaches to multi-phase crystal growth use multi-phase field models and we refer to [22, 21, 30, 13, 34] for a detailed discussion of such models. In [22, 21] formally matched asymptotic expansions are used to relate sharp interface models of the form (1.1) to multi-phase field models. Let us briefly review the literature on numerical methods for multi-phase Mullins–Sekerka problems. To the best of our knowledge, the only front tracking methods for Mullins–Sekerka flows involving several phases and interfaces meeting at triple junctions can be found in [18] and [19], both by the present authors. The model approximated in [18] is based on [12] and is closely related to (1.1), whereas the model considered in [19] is based on the formulation proposed in [24]. Via formally matched asymptotics, the problem (1.1), as well as the models studied in [18, 19], can be recovered as sharp interface limits of certain multi-component viscous Cahn–Hilliard equations. We refer to [12, 22] for details on how to use the method of formally matched asymptotic expansions for Cahn–Hilliard systems. In particular, in [22] the anisotropic force balance condition (1.1e) has been derived. For numerical methods for the approximation of Cahn–Hilliard systems we refer to [20, 11, 2, 31, 28]. Later, we will also discuss some application to snow crystal growth and refer to [29] for an introduction

to the physics of snow crystal growth, to [9] for sharp interface computations for snow crystal growth and to [17] for phase field computations of growing snow crystals.

The rest of the paper is organized as follows. In Section 2, we give the precise mathematical definitions needed to formulate (1.1) and prove a dissipation property of the anisotropic surface energy for solutions of (1.1). In Section 3, we introduce a weak formulation of the system and show the energy bound using this formulation. In Section 4, we propose a fully discrete finite element scheme for the weak formulation introduced in Section 3. We also prove the existence and uniqueness of solutions, as well as an unconditional stability bound that mimics the dissipation property presented in Section 2 on the discrete level. Section 5 is devoted to discussing solution methods for the linear systems that arise at each time level. Finally, we show several numerical simulations in Section 6.

2 Mathematical formulation

In this section, we give the precise definitions needed to formulate the moving boundary problem (1.1). In addition, we present an important property of strong solutions to (1.1).

We begin with the description of the surface cluster $\Gamma(t)$, following the representation of evolving surface clusters from [23] (see also [18]). The domain Ω is split into subdomains $\mathcal{R}_\ell[\Gamma(t)]$ ($\ell \in \mathbb{N}_{\leq I_R}$), with $I_R \geq 2$, by the surface cluster $\Gamma(t) = \bigcup_{i=1}^{I_S} \Gamma_i(t)$, i.e., $\Omega = \Gamma(t) \cup \bigcup_{\ell=1}^{I_R} \mathcal{R}_\ell[\Gamma(t)]$ with $\mathcal{R}_{\ell_1}[\Gamma(t)] \cap \mathcal{R}_{\ell_2}[\Gamma(t)] = \emptyset$ if $\ell_1 \neq \ell_2$. Each $\Gamma_i(t)$ ($i \in \mathbb{N}_{\leq I_S}$) is either a closed hypersurface without boundary or a hypersurface with boundary in Ω . For $k \in \mathbb{N}_{\leq I_T}$, $I_T \geq 0$, let $\mathcal{T}_k(t)$ denote the triple junction at which the three hypersurfaces $\Gamma_{s_1^k}(t)$, $\Gamma_{s_2^k}(t)$ and $\Gamma_{s_3^k}(t)$ with $1 \leq s_1^k < s_2^k < s_3^k \leq I_S$ meet, that is $\mathcal{T}_k(t) \subset \bigcap_{j=1}^3 \partial\Gamma_{s_j^k}(t)$. In addition, $\vec{\mu}_i$ denotes the conormal, i.e. the intrinsic outer unit normal to $\partial\Gamma_i$, the boundary of Γ_i , that lies within the tangent plane of Γ_i . See Figure 1 for an example of a curve network in the three-phase case.

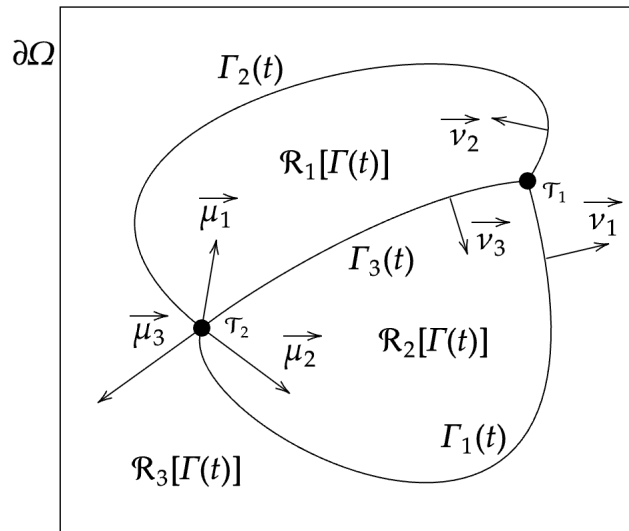


Figure 1: A surface cluster in 2D made up of three open curves and two triple junctions ($d = 2$, $I_S = 3$, $I_R = 3$, $I_T = 2$).

The surface cluster is endowed with the anisotropic surface energy

$$|\Gamma(t)|_\gamma := \sum_{i=1}^{I_S} |\Gamma_i(t)|_{\gamma_i} \quad \text{with} \quad |\Gamma_i(t)|_{\gamma_i} := \int_{\Gamma_i(t)} \gamma_i(\vec{\nu}_i) \, d\mathcal{H}^{d-1}, \quad (2.1)$$

where \mathcal{H}^{d-1} is the $(d-1)$ -dimensional Hausdorff measure. Moreover, $\gamma_i : \mathbb{R}^d \rightarrow \mathbb{R}_{\geq 0}$ ($i \in \mathbb{N}_{\leq I_S}$) denotes the anisotropy function of the surface $\Gamma_i(t)$, which is assumed to be convex and absolutely homogeneous of degree one, i.e., $\gamma_i(\lambda \vec{p}) = |\lambda| \gamma_i(\vec{p})$ for all $\lambda \in \mathbb{R}$ and $\vec{p} \in \mathbb{R}^d$. We assume, that $\gamma_i \in C^1(\mathbb{R}^d \setminus \{0\}, \mathbb{R}_{>0})$, $i \in \mathbb{N}_{\leq I_S}$. Clearly, in the isotropic case $\gamma_i(\vec{p}) = |\vec{p}|$, $i \in \mathbb{N}_{\leq I_S}$, the energy (2.1) reduces to the total surface area of the cluster $\Gamma(t)$.

The anisotropic mean curvature $\kappa_{\gamma,i}$ ($i \in \mathbb{N}_{\leq I_S}$) of $\Gamma_i(t)$ in the direction of $\vec{\nu}_i$ is then defined through the Cahn–Hoffman vector field (see [26]) as follows:

$$\kappa_{\gamma,i} := -\nabla_s \cdot (\gamma_i'(\vec{\nu}_i)) \quad \text{for } i \in \mathbb{N}_{\leq I_S}, \quad (2.2)$$

where $\nabla_s \cdot$ denotes the surface divergence on Γ_i , and γ_i' denotes the spatial gradient of the function $\gamma_i : \mathbb{R}^d \rightarrow \mathbb{R}$. As the γ_i and the β_i are even, we observe that the system (1.1) does not depend on the choice of the normals ν_i on Γ_i .

Similarly to [12, 18], from now on we assume that the chemical potential \mathbf{w} takes values on the hyperplane $T\Sigma := \{\mathbf{u} \in \mathbb{R}^{I_R} \mid \mathbf{u} \cdot \mathbf{1} = \sum_{\ell=1}^{I_R} u_\ell = 0\}$, where $\mathbf{1} = (1, \dots, 1)^\top$. This can be motivated as follows. Taking the inner products of (1.1a), (1.1b), (1.1d), (1.1f) and (1.1g) with $\mathbf{1}$, and noting that $\chi \cdot \mathbf{1} \equiv 0$, we obtain, in a suitable weak sense, that

$$\Delta(\mathbf{w} \cdot \mathbf{1}) = 0 \quad \text{in } \Omega, \quad \nabla_{\vec{\nu}_\Omega}(\mathbf{w} \cdot \mathbf{1}) = 0 \quad \text{on } \partial\Omega_N, \quad \mathbf{w} \cdot \mathbf{1} = \mathbf{w}_D \cdot \mathbf{1} \quad \text{on } \partial\Omega_D.$$

Hence $\mathbf{w} \cdot \mathbf{1}$ is equal to a constant in Ω , which equals $\mathbf{w}_D \cdot \mathbf{1}$ if $\partial\Omega_D \neq \emptyset$. From now on we make the assumption that $\mathbf{w}_D \cdot \mathbf{1} = 0$, i.e. that $\mathbf{w}_D = (w_{D,1}, \dots, w_{D,I_R})^\top \in T\Sigma$, which implies that $\mathbf{w}(\cdot, t) \in T\Sigma$ for $t \in [0, T]$. Furthermore, without loss of generality, we set $\mathbf{w}_D = \mathbf{0}$ if $\partial\Omega_D = \emptyset$.

We note that in the case of the curve network displayed in Figure 1, and for the isotropic surface energy densities $\gamma_i(\vec{p}) = \varsigma_i |\vec{p}|$ with $\varsigma_i > 0$, together with $\rho_i = 0$, for $i = 1, 2, 3$, and $\partial\Omega_N = \partial\Omega$, the system (1.1) collapses to the model (1.2) in [18] which was introduced in [12]. In that paper, the present authors introduced a numerical method based on the parametric finite element method (PFEM) for the numerical approximation of (1.1) in 2D in this simplified setting. Hence the present contribution can be viewed as a generalization of that numerical method, and its analysis, to general surface clusters in 3D with anisotropic surface energies and the presence of kinetic undercooling as well as undercooling imposed at the boundary.

Proposition 2.1. *Assume that $(\mathbf{w}(\cdot, t), \Gamma(t))_{t \in [0, T]}$ is a classical solution to (1.1). Then, we have that*

$$\frac{d}{dt} \left\{ |\Gamma(t)|_\gamma - \sum_{\ell=1}^{I_R} w_{D,\ell} \text{vol}(\mathcal{R}_\ell[\Gamma(t)]) \right\} + \|\nabla \mathbf{w}\|_{L^2(\Omega)}^2 + \left\| \sqrt{\frac{\rho}{\beta(\vec{\nu})}} V \right\|_{L^2(\Gamma(t))}^2 = 0, \quad (2.3)$$

recall (2.1). In addition, it holds that

$$\frac{d}{dt} \text{vol}(\mathcal{R}_\ell[\Gamma(t)]) = \int_{\partial\Omega_D} \nabla w_\ell \cdot \vec{\nu}_\Omega \, d\mathcal{H}^{d-1} \quad \text{for } \ell \in \mathbb{N}_{\leq I_R}. \quad (2.4)$$

Proof. First, we recall from [8, Lemma 3.1 and Eq.(3.4)] that the balance law (1.1e) on the triple junctions implies

$$\frac{d}{dt} \sum_{i=1}^{I_S} |\Gamma_i(t)|_{\gamma_i} = - \sum_{i=1}^{I_S} \int_{\Gamma_i(t)} \kappa_{\gamma,i} V_i \, d\mathcal{H}^{d-1}, \quad (2.5)$$

see also [4, p. 298]. Using (1.1c) and (1.1d), we then obtain that

$$\begin{aligned} \frac{d}{dt} \sum_{i=1}^{I_S} |\Gamma_i(t)|_{\gamma_i} &= - \sum_{i=1}^{I_S} \int_{\Gamma_i(t)} \left(\mathbf{w} \cdot [\chi]_{\Gamma_i} + \frac{\rho_i V_i}{\beta_i(\vec{\nu}_i)} \right) V_i \, d\mathcal{H}^{d-1} \\ &= - \sum_{i=1}^{I_S} \int_{\Gamma_i(t)} \mathbf{w} \cdot (V_i [\chi]_{\Gamma_i}) \, d\mathcal{H}^{d-1} - \sum_{i=1}^{I_S} \int_{\Gamma_i(t)} \frac{\rho_i}{\beta_i(\vec{\nu}_i)} V_i^2 \, d\mathcal{H}^{d-1} \\ &= \sum_{i=1}^{I_S} \int_{\Gamma_i(t)} \mathbf{w} \cdot ([\nabla \mathbf{w}]_{\Gamma_i} \vec{\nu}_i) \, d\mathcal{H}^{d-1} - \sum_{i=1}^{I_S} \int_{\Gamma_i(t)} \frac{\rho_i}{\beta_i(\vec{\nu}_i)} V_i^2 \, d\mathcal{H}^{d-1}. \end{aligned} \quad (2.6)$$

Meanwhile, for each $\ell \in \mathbb{N}_{\leq I_R}$, it follows from integration by parts, (1.1a), (1.1f), and (1.1g) that

$$\begin{aligned} \int_{\Omega} |\nabla w_{\ell}|^2 \, d\mathcal{L}^d &= \int_{\Omega \setminus \Gamma(t)} |\nabla w_{\ell}|^2 \, d\mathcal{L}^d \\ &= \int_{\partial\Omega_D} w_{D,\ell} \nabla w_{\ell} \cdot \vec{\nu}_{\Omega} \, d\mathcal{H}^{d-1} - \sum_{i=1}^{I_S} \int_{\Gamma_i(t)} w_{\ell} [\nabla w_{\ell}]_{\Gamma_i} \cdot \vec{\nu}_i \, d\mathcal{H}^{d-1}. \end{aligned} \quad (2.7)$$

Summing (2.7) for $\ell \in \mathbb{N}_{\leq I_R}$, we have

$$\|\nabla \mathbf{w}\|_{L^2(\Omega)}^2 = \int_{\partial\Omega_D} \mathbf{w}_D \cdot (\nabla \mathbf{w} \vec{\nu}_{\Omega}) \, d\mathcal{H}^{d-1} - \sum_{i=1}^{I_S} \int_{\Gamma_i(t)} \mathbf{w} \cdot ([\nabla \mathbf{w}]_{\Gamma_i} \vec{\nu}_i) \, d\mathcal{H}^{d-1}. \quad (2.8)$$

Similarly to (2.7), we obtain from (1.1a), integration by parts and (1.1d), (1.1g) that

$$\begin{aligned} 0 &= \int_{\Omega \setminus \Gamma(t)} \Delta w_{\ell} \, d\mathcal{L}^d = \int_{\partial\Omega_D} \nabla w_{\ell} \cdot \vec{\nu}_{\Omega} \, d\mathcal{H}^{d-1} - \sum_{i=1}^{I_S} \int_{\Gamma_i(t)} [\nabla w_{\ell}]_{\Gamma_i} \cdot \vec{\nu}_i \, d\mathcal{H}^{d-1} \\ &= \int_{\partial\Omega_D} \nabla w_{\ell} \cdot \vec{\nu}_{\Omega} \, d\mathcal{H}^{d-1} + \sum_{i=1}^{I_S} \int_{\Gamma_i(t)} [\chi_{\ell}]_{\Gamma_i} V_i \, d\mathcal{H}^{d-1} \\ &= \int_{\partial\Omega_D} \nabla w_{\ell} \cdot \vec{\nu}_{\Omega} \, d\mathcal{H}^{d-1} - \frac{d}{dt} \text{vol}(\mathcal{R}_{\ell}[\Gamma(t)]), \end{aligned} \quad (2.9)$$

where we recall that χ_{ℓ} denotes the characteristic function of the region $\mathcal{R}_{\ell}[\Gamma(t)]$, so that $[\chi_{\ell}]_{\Gamma_i} = 1$ if $\Gamma_i(t) \subset \partial\mathcal{R}_{\ell}[\Gamma(t)]$ and $\vec{\nu}_i$ points into the region. This proves (2.4). Moreover, multiplying (2.9) with $w_{D,\ell}$ and summing over $\ell \in \mathbb{N}_{\leq I_R}$ gives

$$\frac{d}{dt} \sum_{\ell=1}^{I_R} w_{D,\ell} \text{vol}(\mathcal{R}_{\ell}[\Gamma(t)]) = \int_{\partial\Omega_D} \mathbf{w}_D \cdot (\nabla \mathbf{w} \vec{\nu}_{\Omega}) \, d\mathcal{H}^{d-1}. \quad (2.10)$$

Combining (2.6), (2.8), and (2.10) yields the desired result (2.3). \square

Remark 2.2. We note that (2.3) gives a dissipation result for the quantity

$$|\Gamma(t)|_{\gamma} - \sum_{\ell=1}^{I_R} w_{D,\ell} \text{vol}(\mathcal{R}_{\ell}[\Gamma(t)]). \quad (2.11)$$

In the case $\partial\Omega_D = \emptyset$ this reduces to the surface energy (2.1). Moreover, if $\partial\Omega_D = \emptyset$, then (2.4) ensures that the volume of each region is preserved. Compare also with Propositions 2.1 and 2.2 in [18].

3 Weak formulation

Let us derive a weak formulation for (1.1). First, we introduce the following function spaces for the bulk trial and test functions:

$$\begin{aligned} \mathbf{S}_0(\Omega) &:= \{u \in H^1(\Omega) \mid u = 0 \text{ on } \partial\Omega_D\}, & \mathbf{S}_0(\Omega) &:= [S_0(\Omega)]^{I_R}, \\ \mathbf{S}_D(\Omega) &:= \{\mathbf{u} \in [H^1(\Omega)]^{I_R} \mid \mathbf{u} = \mathbf{w}_D \text{ on } \partial\Omega_D\}, \\ \mathbf{S}_{\Sigma}(\Omega) &:= \{\mathbf{u} \in [H^1(\Omega)]^{I_R} \mid \mathbf{u}(x) \in T\Sigma \quad \forall x \in \Omega\}. \end{aligned}$$

We suppose that $(\mathbf{w}(\cdot, t), \Gamma(t))_{t \in [0, T]}$ is a solution to (1.1) and $\mathbf{w}(\cdot, t)$ belongs to $\mathbf{S}_D(\Omega) \cap \mathbf{S}_{\Sigma}(\Omega)$. Then, similarly to (2.9), we obtain on testing (1.1a) with $\varphi \in \mathbf{S}_0(\Omega)$ and performing integration by parts,

for $\ell \in \mathbb{N}_{\leq I_R}$ that

$$\begin{aligned} 0 &= \int_{\Omega \setminus \Gamma(t)} \Delta w_\ell \varphi_\ell \, d\mathcal{L}^d = - \sum_{i=1}^{I_S} \int_{\Gamma_i(t)} [\nabla w_\ell]_{\Gamma_i} \cdot \vec{\nu}_i \varphi_\ell \, d\mathcal{H}^{d-1} - \int_{\Omega} \nabla w_\ell \cdot \nabla \varphi_\ell \, d\mathcal{L}^d \\ &= \sum_{i=1}^{I_S} \int_{\Gamma_i(t)} [\chi_\ell]_{\Gamma_i} V_i \varphi_\ell \, d\mathcal{H}^{d-1} - \int_{\Omega} \nabla w_\ell \cdot \nabla \varphi_\ell \, d\mathcal{L}^d, \end{aligned}$$

where we have used that $\varphi_\ell \in \mathcal{S}_0(\Omega)$ and the conditions (1.1f) and (1.1d). Summing over $\ell = 1, \dots, I_R$ gives

$$\int_{\Omega} \nabla \mathbf{w} : \nabla \boldsymbol{\varphi} \, d\mathcal{L}^d - \sum_{\ell=1}^{I_R} \sum_{i=1}^{I_S} \int_{\Gamma_i(t)} [\chi_\ell]_{\Gamma_i} V_i \varphi_\ell \, d\mathcal{H}^{d-1} = 0 \quad \forall \boldsymbol{\varphi} \in \mathcal{S}_0(\Omega). \quad (3.1)$$

We now want to demonstrate that it is enough to choose test functions $\boldsymbol{\varphi} \in \mathcal{S}_0(\Omega) \cap \mathcal{S}_\Sigma(\Omega)$. In fact, choosing in (3.1) a test function $\boldsymbol{\varphi} = \zeta \mathbf{1}$ yields for the first term

$$\int_{\Omega} \sum_{\ell=1}^{I_R} \nabla w_\ell \cdot \nabla \zeta \, d\mathcal{L}^d = \int_{\Omega} \nabla \left(\sum_{\ell=1}^{I_R} w_\ell \right) \cdot \nabla \zeta \, d\mathcal{L}^d = 0,$$

where the last identity holds because $\mathbf{w}(\cdot, t)$ belongs to $\mathcal{S}_\Sigma(\Omega)$. In addition, we also have

$$\sum_{\ell=1}^{I_R} \sum_{i=1}^{I_S} \int_{\Gamma_i(t)} [\chi_\ell]_{\Gamma_i} V_i \zeta \, d\mathcal{H}^{d-1} = \sum_{i=1}^{I_S} \int_{\Gamma_i(t)} \left[\sum_{\ell=1}^{I_R} \chi_\ell \right]_{\Gamma_i} V_i \zeta \, d\mathcal{H}^{d-1} = 0,$$

where the last identity holds because $\sum_{\ell=1}^{I_R} \chi_\ell = 1$. This shows that it is enough to require (3.1) just for test functions $\boldsymbol{\varphi} \in \mathcal{S}_0(\Omega) \cap \mathcal{S}_\Sigma(\Omega)$. Multiplying (1.1c) with a test function $\xi \in L^2(\Gamma(t))$ and integrating over $\Gamma(t)$ yields

$$\sum_{i=1}^{I_S} \int_{\Gamma_i(t)} \kappa_{\gamma_i} \xi_i \, d\mathcal{H}^{d-1} - \sum_{\ell=1}^{I_R} \sum_{i=1}^{I_S} \int_{\Gamma_i(t)} [\chi_\ell]_{\Gamma_i} w_\ell \xi_i \, d\mathcal{H}^{d-1} - \int_{\Gamma_i} \frac{\rho_i}{\beta_i(\vec{\nu}_i)} V_i \xi_i \, d\mathcal{H}^{d-1} = 0. \quad (3.2)$$

For general anisotropies it is not straightforward to come up with a weak formulation of the anisotropic mean curvature vector that is suitable for a parametric finite element approximation based on linear elements. Hence from now on we follow [4, 5, 8, 6] and choose a special class of anisotropies γ_i that are of the form

$$\gamma_i(\vec{p}) = \sum_{\ell=1}^{L_i} \gamma_i^{(\ell)}(\vec{p}), \quad \text{with} \quad \gamma_i^{(\ell)}(\vec{p}) := \sqrt{\vec{p} \cdot G_i^{(\ell)} \vec{p}},$$

where $G_i^{(\ell)} \in \mathbb{R}^{d \times d}$ is a positive definite matrix for each $\ell \in \mathbb{N}_{\leq L_i}$, and $L_i \geq 1$.

We now present a weak formulation of the anisotropic mean curvature vector, which goes back to [5], see also [8] for the extension to surface clusters. We also refer to [27] for an alternative weak formulation. For a symmetric positive matrix G , we set $\tilde{G} = [\det G]^{\frac{1}{d-1}} [G]^{-1}$ and define the \tilde{G} -inner product

$$(\vec{\eta}, \vec{\zeta})_{\tilde{G}} = \vec{\eta} \cdot \tilde{G} \vec{\zeta}, \quad \forall \vec{\eta}, \vec{\zeta} \in \mathbb{R}^d.$$

For a smooth scalar field g over $\Gamma_i(t)$, we define the anisotropic surface gradient

$$\nabla_s^{\tilde{G}} g = \sum_{j=1}^{d-1} \partial_{\vec{t}_j} g \vec{t}_j = \sum_{j=1}^{d-1} (\nabla_s g \cdot \vec{t}_j) \vec{t}_j,$$

where $\partial_{\vec{t}_j} g = \nabla_s g \cdot \vec{t}_j$ is the directional derivative, ∇_s is the usual surface gradient operator, and $\{\vec{t}_j\}_{j=1}^{d-1}$ forms an orthonormal basis with respect to the \tilde{G} -inner product for the tangent plane of $\Gamma_i(t)$ at the point of interest, i.e.,

$$\vec{t}_j \cdot \vec{v}_i = 0, \quad (\vec{t}_j, \vec{t}_k)_{\tilde{G}} = \delta_{jk}, \quad 1 \leq j, k \leq d-1.$$

Moreover, the anisotropic surface divergence and gradient of a smooth vector field \vec{g} are given by

$$\nabla_s^{\tilde{G}} \cdot \vec{g} = \sum_{j=1}^{d-1} (\partial_{\vec{t}_j} \vec{g}) \cdot (\tilde{G} \vec{t}_j), \quad \nabla_s^{\tilde{G}} \vec{g} = \sum_{j=1}^{d-1} (\partial_{\vec{t}_j} \vec{g}) \otimes (\tilde{G} \vec{t}_j),$$

where \otimes is the standard tensor product for two vectors in \mathbb{R}^d . We also define the inner product

$$(\nabla_s^{\tilde{G}} \vec{u}, \nabla_s^{\tilde{G}} \vec{v})_{\tilde{G}} := \sum_{i=1}^{d-1} (\partial_{\vec{t}_i} \vec{u}, \partial_{\vec{t}_i} \vec{v})_{\tilde{G}} \quad (3.3)$$

for smooth $\vec{u}, \vec{v} : \Gamma \rightarrow \mathbb{R}^d$. Then, we define for smooth functions $\vec{\eta}$ and $\vec{\zeta}$ the inner product

$$\langle \nabla_s^{\tilde{G}} \vec{\eta}, \nabla_s^{\tilde{G}} \vec{\zeta} \rangle_{\gamma, \Gamma(t)} = \sum_{i=1}^{I_S} \sum_{\ell=1}^{L_i} \int_{\Gamma_i(t)} \left(\nabla_s^{\tilde{G}_i^{(\ell)}} \vec{\eta}, \nabla_s^{\tilde{G}_i^{(\ell)}} \vec{\zeta} \right)_{\tilde{G}_i^{(\ell)}} \gamma_\ell(\vec{v}_i) \, d\mathcal{H}^{d-1}. \quad (3.4)$$

In [8] it was shown that for a surface cluster satisfying (1.1e) the anisotropic mean curvature (2.2) satisfies the identity

$$\sum_{i=1}^{I_S} \int_{\Gamma_i(t)} \kappa_{\gamma, i} \vec{v}_i \cdot \vec{\eta}_i \, d\mathcal{H}^{d-1} + \langle \nabla_s^{\tilde{G}} \text{id}, \nabla_s^{\tilde{G}} \vec{\eta} \rangle_{\gamma, \Gamma(t)} = 0$$

for every $\vec{\eta} \in [H^1(\Gamma(t))]^d$ with $\vec{\eta}_{s_i^k} = \vec{\eta}_{s_2^k} = \vec{\eta}_{s_3^k}$ on \mathcal{T}_k , for all $k \in \mathbb{N}_{\leq I_T}$.

Let us summarize the weak formulation of the system (1.1) as follows. Here for convenience we let $\langle \cdot, \cdot \rangle_\Omega$ denote the L^2 -inner product over Ω , and similarly for $\Gamma_i(t)$ as well as $\langle \cdot, \cdot \rangle_{\Gamma(t)} = \sum_{i=1}^{I_S} \langle \cdot, \cdot \rangle_{\Gamma_i(t)}$. Find $(\mathbf{w}, \Gamma(t))_{t \in [0, T]}$ such that $\Gamma(0) = \Gamma_0$ and for all $t \in (0, T]$ it holds that $\mathbf{w}(t) \in \mathbf{S}_D(\Omega) \cap \mathbf{S}_\Sigma(\Omega)$ such that the following identities hold.

[Motion law] For all $\varphi \in \mathbf{S}_0(\Omega) \cap \mathbf{S}_\Sigma(\Omega)$,

$$\langle \nabla \mathbf{w}, \nabla \varphi \rangle_\Omega - \sum_{\ell=1}^{I_R} \sum_{i=1}^{I_S} \left\langle [\chi_\ell]_{\Gamma_i} V_i, \varphi_\ell \right\rangle_{\Gamma_i(t)} = 0. \quad (3.5a)$$

[Gibbs–Thomson law with kinetic undercooling] For all $\xi \in L^2(\Gamma(t))$,

$$\langle \kappa_\gamma, \xi \rangle_{\Gamma(t)} - \sum_{\ell=1}^{I_R} \sum_{i=1}^{I_S} \left\langle [\chi_\ell]_{\Gamma_i} w_\ell, \xi_i \right\rangle_{\Gamma_i(t)} - \left\langle \frac{\rho}{\beta(\vec{v})} V, \xi \right\rangle_{\Gamma(t)} = 0. \quad (3.5b)$$

[Curvature vector] For all $\vec{\eta} \in [H^1(\Gamma(t))]^d$ such that $\vec{\eta}_{s_1^k} = \vec{\eta}_{s_2^k} = \vec{\eta}_{s_3^k}$ on $\mathcal{T}_k(t)$ for every $k \in \mathbb{N}_{\leq I_T}$,

$$\langle \kappa_\gamma \vec{v}, \vec{\eta} \rangle_\Gamma + \left\langle \nabla_s^{\tilde{G}} \text{id}, \nabla_s^{\tilde{G}} \vec{\eta} \right\rangle_{\gamma, \Gamma(t)} = 0. \quad (3.5c)$$

4 Finite element approximation

Let the time interval $[0, T]$ be split into M sub-intervals $[t_{m-1}, t_m]$ for each $m = 1, \dots, M$, whose length are equal to τ_m . Then, given a multiplet of polygonal surfaces $\Gamma^0 = (\Gamma_1^0, \dots, \Gamma_{I_S}^0)$, our aim is to find time discrete multiplets $\Gamma^1, \dots, \Gamma^M$ governed by discrete analogues of (3.5).

Let us first define the finite element spaces from where we will seek the approximate solutions. Let \mathcal{T}^m be a triangulation of $\bar{\Omega}$.

$$\begin{aligned} S^m &:= \{v \in C(\bar{\Omega}) \mid v|_o \text{ is affine } \forall o \in \mathcal{T}^m\}, & \mathbf{S}^m &:= [S^m]^{I_R}, \\ S_0^m &:= \{v \in S^m \mid v = \mathbf{0} \text{ on } \partial\Omega_D\}, & S_D^m &:= \{v \in S^m \mid v = \mathbf{w}_D \text{ on } \partial\Omega_D\}, \\ S_\Sigma^m &:= \{v \in S^m \mid v(x) \in T\Sigma \quad \forall x \in \bar{\Omega}\}. \end{aligned}$$

Using these notations, the discrete chemical potential \mathbf{W}^{m+1} will be sought in $S_D^m \cap S_\Sigma^m$.

For the following presentation of the discrete surface clusters we closely follow the presentation in [8], see also [1] and [19]. In order to describe Γ^m for $m \geq 0$, and the discrete matching conditions that have to hold on the triple junction, we let Υ_i^h ($i \in \mathbb{N}_{\leq I_S}$) be polyhedral reference surfaces with $\bar{\Upsilon}_i^h = \bigcup_{j=1}^{J_i} \bar{\sigma}_{i,j}$, where $\{\sigma_{i,j}\}_{j=1}^{J_i}$ is a family of mutually disjoint open $(d-1)$ -simplices with vertices $\{\vec{q}_{i,k}\}_{k=1}^{K_i}$ vertices.

Moreover, we assume that each boundary $\partial\Upsilon_i^h$ is split into I_p^i sub-boundaries $\partial_p\Upsilon_i^h$ ($p \in \mathbb{N}_{\leq I_p^i}$), and each sub-boundary $\partial_p\Upsilon_i^h$ corresponds to the parameterization of a triple junction. In particular, we will let $\Gamma_i^m = \vec{\mathfrak{X}}_i^m(\Upsilon_i^h)$, so that the triple junction \mathcal{T}_k , where the surfaces $\Gamma_{s_1^k}(t)$, $\Gamma_{s_2^k}(t)$, and $\Gamma_{s_3^k}(t)$ meet, is approximated by the images of $\vec{\mathfrak{X}}^m$ on $\partial_{p_1^k}\Upsilon_{s_1^k}^h$, $\partial_{p_2^k}\Upsilon_{s_2^k}^h$, and $\partial_{p_3^k}\Upsilon_{s_3^k}^h$. To this end, we have to ensure that these sub-boundaries perfectly match up on the triple junctions, and in particular contain the same number of vertices. Hence, we assume that for every $k \in \mathbb{N}_{\leq I_T}$, it holds that

$$Z_k := \#Q_{s_1^k, p_1^k} = \#Q_{s_2^k, p_2^k} = \#Q_{s_3^k, p_3^k}, \quad (4.1)$$

where $Q_{s,p} := \left\{ \vec{q}_{s,\ell} \right\}_{\ell=1}^{K_s} \cap \partial_p\Upsilon_s^h$ denotes the set of vertices belonging to the boundary patch $\partial_p\Upsilon_s^h$. Then we assume in addition that there exist bijections $\vec{\varrho}_r^k : \mathbb{N}_{\leq Z_k} \rightarrow Q_{s_r^k, p_r^k}$ ($r = 1, 2, 3$) such that $(\vec{\varrho}_r^k(1), \dots, \vec{\varrho}_r^k(Z_k))$ ($r = 1, 2, 3$) are ordered sequences of the vertices.

Let

$$\begin{aligned} \underline{V}^h(\Upsilon^h) &:= \left\{ (\vec{\mathfrak{X}}_1, \dots, \vec{\mathfrak{X}}_{I_S}) \in \bigotimes_{i=1}^{I_S} [C(\bar{\Upsilon}_i^h)]^d \mid \vec{\mathfrak{X}}_i|_{\sigma_{i,j}} \text{ is affine } \forall j \in \mathbb{N}_{\leq J_i}, \forall i \in \mathbb{N}_{\leq I_S}, \right. \\ &\quad \left. \text{and } \vec{\mathfrak{X}}_{s_1^k}(\vec{\varrho}_1^k(z)) = \vec{\mathfrak{X}}_{s_2^k}(\vec{\varrho}_2^k(z)) = \vec{\mathfrak{X}}_{s_3^k}(\vec{\varrho}_3^k(z)) \quad \forall z \in \mathbb{N}_{\leq Z_k}, \forall k \in \mathbb{N}_{\leq I_T} \right\}. \end{aligned}$$

Then, for each $m \geq 0$ and $\vec{\mathfrak{X}}^m \in V^h(\Upsilon^h)$, we define $\Gamma^m := \vec{\mathfrak{X}}^m(\Upsilon^h)$ with $\Gamma_i^m = \vec{\mathfrak{X}}_i^m(\Upsilon_i^h)$, $\sigma_{i,j}^m := \vec{\mathfrak{X}}_i^m(\sigma_{i,j})$ and $\vec{q}_{i,k}^m := \vec{\mathfrak{X}}_i^m(\vec{q}_{i,k})$. The discrete triple junctions \mathcal{T}_k^m ($k \in \mathbb{N}_{\leq I_T}$) are defined by $\mathcal{T}_k^m := \left\{ \vec{\mathfrak{X}}_{s_1^k}^m(\vec{\varrho}_1^k(z)) \mid z \in \mathbb{N}_{\leq Z_k} \right\}$. On the polyhedral surface Γ^m , we introduce finite element spaces defined by

$$V^h(\Gamma_i^m) := \left\{ v \in C(\Gamma_i^m) \mid v|_{\sigma_{i,j}^m} \text{ is affine } \forall j \in \mathbb{N}_{\leq J_i} \right\}, \quad \underline{V}^h(\Gamma_i^m) := [V^h(\Gamma_i^m)]^d, \quad i \in \mathbb{N}_{\leq I_S}.$$

For later use, we also define

$$V_0^h(\Gamma_i^m) := \{v \in V^h(\Gamma_i^m) \mid v = 0 \text{ on } \partial\Gamma_i^m\}, \quad \underline{V}_0^h(\Gamma_i^m) := [V_0^h(\Gamma_i^m)]^d, \quad i \in \mathbb{N}_{\leq I_S} \quad (4.2)$$

and let $\{\Phi_{i,k}^{m,0}\}_{k=1}^{K_i^0}$ be the standard basis of $V_0^h(\Gamma_i^m)$, so that $\Phi_{i,k}^{m,0}(\vec{q}_{i,\ell}^m) = \delta_{k\ell}$, $k, \ell \in \mathbb{N}_{\leq K_i^0}$.

Then, the approximate solutions \vec{X}^{m+1} and κ_γ^{m+1} are respectively sought in the finite element spaces defined by

$$\begin{aligned} \underline{V}_{\mathcal{T}}^h(\Gamma^m) &:= \left\{ (\vec{X}_1, \dots, \vec{X}_{I_S}) \in \bigotimes_{i=1}^{I_S} \underline{V}^h(\Gamma_i^m) \mid \vec{X}_{s_1^k} = \vec{X}_{s_2^k} = \vec{X}_{s_3^k} \text{ on } \mathcal{T}_k^m, \forall k \in \mathbb{N}_{\leq I_T} \right\}, \\ V^h(\Gamma^m) &:= \bigotimes_{i=1}^{I_S} V^h(\Gamma_i^m). \end{aligned}$$

We now define the normal vector of each simplex $\sigma_{i,j}^m$. To this end, let $\{\bar{q}_{i,j,\ell}^m\}_{\ell=1}^d$ be the vertices of $\sigma_{i,j}^m$, and ordered with the same orientation for all $\sigma_{i,j}^m$, $j \in \mathbb{N}_{\leq J_i}$. Then we define

$$\vec{\nu}_{i,j}^m := \frac{\vec{A}\{\sigma_{i,j}^m\}}{|\vec{A}\{\sigma_{i,j}^m\}|} \quad \text{with} \quad \vec{A}\{\sigma_{i,j}^m\} := \begin{cases} (\bar{q}_{i,j,2}^m - \bar{q}_{i,j,1}^m)^\perp & \text{if } d = 2, \\ (\bar{q}_{i,j,2}^m - \bar{q}_{i,j,1}^m) \wedge (\bar{q}_{i,j,3}^m - \bar{q}_{i,j,1}^m) & \text{if } d = 3, \end{cases}$$

where $|\cdot| = \mathcal{H}^{d-1}(\cdot)$; the symbol \wedge denotes the wedge product, and $v^\perp := (-v_2, v_1)^\top$ for $v = (v_1, v_2)^\top \in \mathbb{R}^2$. Let $\vec{\nu}_i^m$ be the normal vector on Γ_i^m which equals $\vec{\nu}_{i,j}^m$ on $\sigma_{i,j}^m$.

Let us define the mass lumped inner product of two piecewise continuous functions u and v on Γ_i^m by

$$\langle u, v \rangle_{\Gamma_i^m}^h := \frac{1}{d} \sum_{j=1}^{J_i} |\sigma_{i,j}^m| \sum_{k=1}^d \lim_{\sigma_{i,j}^m \ni \bar{q} \rightarrow \bar{q}_{i,j,k}^m} (uv)(\bar{q}), \quad i \in \mathbb{N}_{\leq I_S}.$$

Using this, we define the mass lumped inner product on Γ^m by

$$\langle u, v \rangle_{\Gamma^m}^h := \sum_{i=1}^{I_S} \langle u_i, v_i \rangle_{\Gamma_i^m}^h.$$

Meanwhile, we will write the natural L^2 -inner product as follows:

$$\langle u, v \rangle_{\Gamma^m} = \sum_{i=1}^{I_S} \langle u_i, v_i \rangle_{\Gamma_i^m} = \sum_{i=1}^{I_S} \int_{\Gamma_i^m} u_i v_i \, d\mathcal{H}^{d-1}.$$

The notion of these inner products can be extended for two vector- and tensor-valued functions. The vertex normal $\vec{\omega}_i^m \in \underline{V}^h(\Gamma_i^m)$ on Γ_i^m is defined in terms of the L^2 -projection as follows (see [10]):

$$\langle \vec{\omega}_i^m, \vec{\xi} \rangle_{\Gamma_i^m}^h = \langle \vec{\nu}_i^m, \vec{\xi} \rangle_{\Gamma_i^m}^h, \quad \forall \vec{\xi} \in \underline{V}^h(\Gamma_i^m), \quad i \in \mathbb{N}_{\leq I_S}.$$

Our finite element approximation of (3.5) is now given as follows. Let Γ^0 be given. Then, for $m \geq 0$, find $(\mathbf{W}^{m+1}, \kappa_\gamma^{m+1}, \vec{X}^{m+1}) \in (\mathbf{S}_D^m \cap \mathbf{S}_\Sigma^m) \times V^h(\Gamma^m) \times \underline{V}_\mathcal{T}^h(\Gamma^m)$, and set $\Gamma^{m+1} = \vec{X}^{m+1}(\Gamma^m)$, such that the following conditions hold:

[Motion law] For all $\varphi \in \mathbf{S}_0^m \cap \mathbf{S}_\Sigma^m$,

$$\langle \nabla \mathbf{W}^{m+1}, \nabla \varphi \rangle_\Omega - \sum_{\ell=1}^{I_R} \sum_{i=1}^{I_S} \left\langle [\chi_\ell]_{\Gamma_i^m} \pi_i^h \left[\frac{\vec{X}_i^{m+1} - \text{id}}{\tau_m} \cdot \vec{\omega}_i^m \right], \varphi_\ell \right\rangle_{\Gamma_i^m}^{(h)} = 0. \quad (4.3a)$$

[Gibbs–Thomson law with kinetic undercooling] For all $\xi \in V^h(\Gamma^m)$,

$$\langle \kappa_\gamma^{m+1}, \xi \rangle_{\Gamma^m}^h - \sum_{\ell=1}^{I_R} \sum_{i=1}^{I_S} \left\langle [\chi_\ell]_{\Gamma_i^m} W_\ell^{m+1}, \xi_i \right\rangle_{\Gamma_i^m}^{(h)} - \left\langle \frac{\rho}{\beta(\vec{\nu}^m)} \frac{\vec{X}^{m+1} - \text{id}}{\tau_m}, \xi \vec{\omega}^m \right\rangle_{\Gamma^m}^h = 0. \quad (4.3b)$$

[Curvature vector] For all $\vec{\eta} \in \underline{V}_\mathcal{T}^h(\Gamma^m)$,

$$\langle \kappa_\gamma^{m+1} \vec{\omega}^m, \vec{\eta} \rangle_{\Gamma^m}^h + \left\langle \nabla_s^{\vec{G}} \vec{X}^{m+1}, \nabla_s^{\vec{G}} \vec{\eta} \right\rangle_{\gamma, \Gamma^m} = 0, \quad (4.3c)$$

where, analogously to (3.4), we have defined the discrete inner product

$$\left\langle \nabla_s^{\vec{G}} \vec{\zeta}, \nabla_s^{\vec{G}} \vec{\eta} \right\rangle_{\gamma, \Gamma^m} := \sum_{i=1}^{I_S} \sum_{\ell=1}^{L_i} \int_{\Gamma_i^m} \left(\nabla_s^{\vec{G}_i^{(\ell)}} \vec{\zeta}_i, \nabla_s^{\vec{G}_i^{(\ell)}} \vec{\eta}_i \right)_{\vec{G}_i^{(\ell)}} \gamma_i^{(\ell)}(\vec{\nu}_i^m) \, d\mathcal{H}^{d-1}.$$

Observe that here and throughout, the notation $\cdot^{(h)}$ means an expression with or without the superscript h . That is, the scheme (4.3) represents two different numerical methods: one with mass lumping in the bulk-interface cross terms in (4.3a) and (4.3b), and one with exact integration. This follows similar approaches in [7, 32, 18, 19].

Our aim is to prove the well-posedness and unconditional stability of the introduced scheme (4.3). For the former we make a mild assumption on the cluster Γ^m , as well as on the compatibility between the bulk triangulation \mathcal{T}^m and Γ^m . This follows analogous assumptions being made in [10, Assumptions 64 and 108], see also [18, 19].

Assumption 1. *For every $i \in \mathbb{N}_{\leq I_S}$, it holds that*

$$\text{span} \left\{ \vec{\omega}_i^m(\vec{q}_{i,k}^m) \mid k \in \mathbb{N}_{\leq K_i^0} \right\} \neq \{\vec{0}\}.$$

Moreover, we assume that

$$\text{span} \left\{ \sum_{\ell=1}^{I_R} \sum_{i=1}^{I_S} \left\langle [\chi_\ell]_{\Gamma_i^m} \vec{\omega}_i^m, \varphi_\ell \right\rangle_{\Gamma_i^m}^{(h)} \mid \varphi \in \mathbf{S}_0^m \cap \mathbf{S}_\Sigma^m \right\} = \mathbb{R}^d. \quad (4.4)$$

We now establish the well-posedness of the finite element approximation (4.3).

Theorem 4.1. *Let \mathcal{T}^m and Γ^m satisfy Assumption 1. Then there exists a unique solution*

$$(\mathbf{W}^{m+1}, \kappa_\gamma^{m+1}, \vec{X}^{m+1}) \in (\mathbf{S}_D^m \cap \mathbf{S}_\Sigma^m) \times V^h(\Gamma^m) \times \underline{V}_{\mathcal{T}}^h(\Gamma^m)$$

to (4.3).

Proof. Since the system (4.3) is linear in the unknowns, with as many unknowns as equations, it suffices to show that $(\mathbf{W}^{m+1}, \kappa_\gamma^{m+1}, \vec{X}^{m+1}) \equiv (\mathbf{0}, 0, \vec{0})$ is the only solution to the homogeneous system of (4.3). Therefore, we assume that $(\mathbf{W}, \kappa_\gamma, \vec{X}) \in (\mathbf{S}_0^m \cap \mathbf{S}_\Sigma^m) \times V^h(\Gamma^m) \times \underline{V}_{\mathcal{T}}^h(\Gamma^m)$ is a solution to

$$\langle \nabla \mathbf{W}, \nabla \varphi \rangle_\Omega - \sum_{\ell=1}^{I_R} \sum_{i=1}^{I_S} \left\langle [\chi_\ell]_{\Gamma_i^m} \pi_i^h \left[\frac{\vec{X}_i}{\tau_m} \cdot \vec{\omega}_i^m \right], \varphi_\ell \right\rangle_{\Gamma_i^m}^{(h)} = 0 \quad \forall \varphi \in \mathbf{S}_0^m \cap \mathbf{S}_\Sigma^m, \quad (4.5a)$$

$$\langle \kappa_\gamma, \xi \rangle_{\Gamma^m}^h - \sum_{\ell=1}^{I_R} \sum_{i=1}^{I_S} \left\langle [\chi_\ell]_{\Gamma_i^m} W_\ell, \xi_i \right\rangle_{\Gamma_i^m}^{(h)} - \left\langle \frac{\rho}{\beta(\vec{\nu}^m)} \frac{\vec{X}}{\tau_m}, \xi \vec{\omega}^m \right\rangle_{\Gamma^m}^h = 0 \quad \forall \xi \in V^h(\Gamma^m), \quad (4.5b)$$

$$\langle \kappa_\gamma \vec{\omega}^m, \vec{\eta} \rangle_{\Gamma^m}^h + \left\langle \nabla_s^{\tilde{G}} \vec{X}, \nabla_s^{\tilde{G}} \vec{\eta} \right\rangle_{\gamma, \Gamma^m} = 0 \quad \forall \vec{\eta} \in \underline{V}_{\mathcal{T}}^h(\Gamma^m). \quad (4.5c)$$

Choosing $\varphi = \mathbf{W}$ in (4.5a), $\xi = \pi^h [\vec{X} \cdot \vec{\omega}^m]$ in (4.5b), and $\vec{\eta} = \vec{X}$ in (4.5c), we obtain

$$\left\langle \nabla_s^{\tilde{G}} \vec{X}, \nabla_s^{\tilde{G}} \vec{X} \right\rangle_{\gamma, \Gamma^m} + \tau_m \|\nabla \mathbf{W}\|_{L^2(\Omega)}^2 + \frac{1}{\tau_m} \left\langle \frac{\rho}{\beta(\vec{\nu}^m)} \vec{X} \cdot \vec{\omega}^m, \vec{X} \cdot \vec{\omega}^m \right\rangle_{\Gamma^m}^h = 0.$$

Since all the terms on the left-hand side of the above equation are non-negative, we can use the fact that all $\tilde{G}_i^{(\ell)}$ are positive definite and the definition (3.3) to conclude that $\mathbf{W} \equiv \mathbf{C} \in T\Sigma$ and $\vec{X} \equiv \vec{X}_c$ are constant functions. If $\partial\Omega_D \neq \emptyset$ we immediately get $\mathbf{C} = \mathbf{0}$. Meanwhile, we deduce from (4.5a) that for any $\varphi \in \mathbf{S}_0^m \cap \mathbf{S}_\Sigma^m$,

$$\vec{X}_c \cdot \sum_{\ell=1}^{I_R} \sum_{i=1}^{I_S} \left\langle [\chi_\ell]_{\Gamma_i^m} \vec{\omega}_i^m, \varphi_\ell \right\rangle_{\Gamma_i^m}^{(h)} = 0.$$

We see from Assumption 1 that the above equation holds if and only if $\vec{X}_c = \vec{0}$. Hence it follows from (4.5b) that

$$\kappa_{\gamma,i} = \sum_{\ell=1}^{I_R} [\chi_\ell]_{\Gamma_i^m} C_\ell \quad (4.6)$$

is also equal to a constant, for $i \in \mathbb{N}_{\leq I_S}$. With these constants, we now define

$$\vec{\eta}_i := \kappa_{\gamma,i} \sum_{j=1}^{K_i^0} \vec{\omega}_i^m(\vec{q}_{i,\ell}^m) \Phi_{i,j}^m \in [V_0^h(\Gamma_i^m)]^d \quad \text{for } i \in \mathbb{N}_{\leq I_S}. \quad (4.7)$$

On recalling (4.2) we observe that $\vec{\eta} = (\vec{\eta}_1, \dots, \vec{\eta}_{I_S}) \in \underline{V}_{\mathcal{T}}^h(\Gamma^m)$. Thus, on choosing this $\vec{\eta}$ in (4.5c) we obtain

$$0 = \langle \kappa_{\gamma} \vec{\omega}^m, \vec{\eta} \rangle_{\Gamma^m}^h = \sum_{i=1}^{I_S} \kappa_{\gamma,i} \langle \vec{\omega}_i^m, \vec{\eta}_i \rangle_{\Gamma_i^m}^h = \sum_{i=1}^{I_S} (\kappa_{\gamma,i})^2 \sum_{j=1}^{K_i^0} |\vec{\omega}_{i,j}^m(\vec{q}_{i,\ell}^m)|^2 \langle \Phi_{i,j}^m, \Phi_{i,j}^m \rangle_{\Gamma_i^m}^h.$$

Assumption 1 now immediately implies that $\kappa_{\gamma,i} = 0$ for $i \in \mathbb{N}_{\leq I_S}$, and hence $\kappa_{\gamma} \equiv 0$. Finally, in view of the fact that Ω is connected, it is not difficult to show that (4.6) together with $\mathbf{C} \in T\Sigma$ implies that $\mathbf{C} = \mathbf{0}$. This concludes the proof. \square

We now show a discrete analogue of the energy dissipation law in Proposition 2.1.

Theorem 4.2 (Discrete energy dissipation). *Let $(\mathbf{W}^{m+1}, \kappa_{\gamma}^{m+1}, \vec{X}^{m+1}) \in (\mathbf{S}_D^m \cap \mathbf{S}_{\Sigma}^m) \times V^h(\Gamma^m) \times \underline{V}_{\mathcal{T}}^h(\Gamma^m)$ be the solution to (4.3). Then, the following inequality holds:*

$$\begin{aligned} & |\Gamma^{m+1}|_{\gamma} + \tau_m \sum_{\ell=1}^{I_R} w_{D,\ell} \sum_{i=1}^{I_S} \left\langle [\chi_{\ell}]_{\Gamma_i^m} \frac{\vec{X}^{m+1} - \text{id}}{\tau_m}, \vec{\omega}_i^m \right\rangle_{\Gamma_i^m}^{(h)} \\ & + \tau_m \|\nabla \mathbf{W}^{m+1}\|_{L^2(\Omega)}^2 + \tau_m \left\langle \frac{\rho}{\beta(\vec{\nu}^m)}, \left| \frac{\vec{X}^{m+1} - \text{id}}{\tau_m} \cdot \vec{\omega}^m \right|^2 \right\rangle_{\Gamma^m}^h \leq |\Gamma^m|_{\gamma}. \end{aligned} \quad (4.8)$$

Proof. Choosing $\varphi = \mathbf{W}^{m+1} - \mathbf{w}_D \in \mathbf{S}_0^m \cap \mathbf{S}_{\Sigma}^m$ in (4.3a), $\xi = \pi^h [(\vec{X}^{m+1} - \text{id})|_{\Gamma^m} \cdot \vec{\omega}^m]$ in (4.3b) and $\vec{\eta} = \vec{X}^{m+1} - \text{id}|_{\Gamma^m}$ in (4.3c) yields that

$$\|\nabla \mathbf{W}^{m+1}\|_{L^2(\Omega)}^2 - \sum_{\ell=1}^{I_R} \sum_{i=1}^{I_S} \left\langle [\chi_{\ell}]_{\Gamma_i^m} \pi_i^h \left[\frac{\vec{X}^{m+1} - \text{id}}{\tau_m} \cdot \vec{\omega}_i^m \right], W_{\ell}^{m+1} - w_{D,\ell} \right\rangle_{\Gamma_i^m}^{(h)} = 0, \quad (4.9a)$$

$$\begin{aligned} & \left\langle \kappa_{\gamma}^{m+1} \vec{\omega}^m, \vec{X}^{m+1} - \text{id} \right\rangle_{\Gamma^m}^h - \sum_{\ell=1}^{I_R} \sum_{i=1}^{I_S} \left\langle [\chi_{\ell}]_{\Gamma_i^m} W_{\ell}^{m+1}, \pi_i^h [(\vec{X}^{m+1} - \text{id}) \cdot \vec{\omega}_i^m] \right\rangle_{\Gamma_i^m}^{(h)} \\ & - \left\langle \frac{\rho}{\beta(\vec{\nu}^m)} \frac{\vec{X}^{m+1} - \text{id}}{\tau_m} \cdot \vec{\omega}^m, (\vec{X}^{m+1} - \text{id}) \cdot \vec{\omega}^m \right\rangle_{\Gamma^m}^h = 0, \end{aligned} \quad (4.9b)$$

$$\left\langle \kappa_{\gamma}^{m+1} \vec{\omega}^m, \vec{X}^{m+1} - \text{id} \right\rangle_{\Gamma^m}^h + \left\langle \nabla_s^{\tilde{G}} \vec{X}^{m+1}, \nabla_s^{\tilde{G}} (\vec{X}^{m+1} - \text{id}) \right\rangle_{\gamma, \Gamma^m} = 0. \quad (4.9c)$$

Combining (4.9a), (4.9b) and (4.9c) yields that

$$\begin{aligned} & \tau_m \|\nabla \mathbf{W}^{m+1}\|_{L^2(\Omega)}^2 + \sum_{\ell=1}^{I_R} \sum_{i=1}^{I_S} \left\langle [\chi_{\ell}]_{\Gamma_i^m} \pi_i^h [(\vec{X}^{m+1} - \text{id}) \cdot \vec{\omega}_i^m], w_{D,\ell} \right\rangle_{\Gamma_i^m}^{(h)} \\ & + \frac{1}{\tau_m} \left\langle \frac{\rho}{\beta(\vec{\nu}^m)}, |(\vec{X}^{m+1} - \text{id}) \cdot \vec{\omega}^m|^2 \right\rangle_{\Gamma^m}^h + \left\langle \nabla_s^{\tilde{G}} \vec{X}^{m+1}, \nabla_s^{\tilde{G}} (\vec{X}^{m+1} - \text{id}) \right\rangle_{\gamma, \Gamma^m} = 0. \end{aligned} \quad (4.10)$$

We now recall the following discrete anisotropic energy estimate from [10, Lemma 102]:

$$\left\langle \nabla_s^{\tilde{G}} \vec{X}^{m+1}, \nabla_s^{\tilde{G}} (\vec{X}^{m+1} - \text{id}) \right\rangle_{\gamma, \Gamma^m} \geq |\Gamma^{m+1}|_{\gamma} - |\Gamma^m|_{\gamma}, \quad (4.11)$$

see also [4, 5]. The desired result (4.8) directly follows from (4.10) and (4.11). \square

Remark 4.3. *It is not difficult to see that (4.8) is a discrete analogue of the dissipation property (2.3). In fact, we only need to recall from (2.9) that*

$$-\frac{d}{dt} \sum_{\ell=1}^{I_R} w_{D,\ell} \text{vol}(\mathcal{R}_\ell[\Gamma(t)]) = \sum_{\ell=1}^{I_R} w_{D,\ell} \sum_{i=1}^{I_S} \int_{\Gamma_i(t)} [\chi_\ell]_{\Gamma_i} V_i \, d\mathcal{H}^{d-1}.$$

Moreover, we note that (4.8) is the natural generalization of the discrete energy estimate [7, Theorem 3.1] to the multi-phase problem considered here.

5 Solution methods

In this section, we discuss solution methods for the system of linear equations arising from (4.3) at each time level. To this end, we make use of ideas from [3, 7], see also [18, 19]. Here the crucial idea is to avoid having to work with the trial and test spaces $\underline{V}_{\mathcal{T}}^h(\Gamma^m)$ and \mathbf{S}_{Σ}^m directly, and rather employ a technique that is similar to a standard treatment of periodic boundary conditions for ODEs and PDEs.

We introduce the orthogonal projections $\mathcal{P} : [V^h(\Gamma^m)]^d \rightarrow \underline{V}_{\mathcal{T}}^h(\Gamma^m)$ and $\mathcal{Q} : \mathbf{S}^m \rightarrow \mathbf{S}_{\Sigma}^m$, where as inner product in each case we consider the mass lumped L^2 -inner product. Firstly, it is easy to see that for $\mathbf{W} \in \mathbf{S}^m$ it holds that $\mathcal{Q}\mathbf{W} = \mathbf{W} - \frac{\mathbf{W} \cdot \mathbf{1}}{\mathbf{1} \cdot \mathbf{1}} \mathbf{1}$ point-wise in $\bar{\Omega}$.

Now, given $\vec{X}^m := \text{id}|_{\Gamma^m} \in \underline{V}_{\mathcal{T}}^h(\Gamma^m)$, let $(\mathbf{W}^{m+1}, \kappa_\gamma^{m+1}, \vec{X}^m + \delta \vec{X}^{m+1}) \in (\mathbf{S}_D^m \cap \mathbf{S}_{\Sigma}^m) \times V^h(\Gamma^m) \times \underline{V}_{\mathcal{T}}^h(\Gamma^m)$ be the unique solution to (4.3) whose existence has been proven in Theorem 4.1. From now on, as no confusion can arise, we identify $(\mathbf{W}^{m+1}, \kappa_\gamma^{m+1}, \delta \vec{X}^{m+1})$ with their vectors of coefficients with respect to the bases $\{\Psi_i^m\}_{1 \leq i \leq K_\Omega^m}$ and $\{\{\Phi_{i,j}^m\}_{1 \leq j \leq N_i}\}_{i=1}^{I_S}$ of the unconstrained spaces \mathbf{S}^m and $V^h(\Gamma^m)$. Let $N = \sum_{i=1}^{I_S} N_i$ and $K = I_R K_\Omega^m$. Then, in addition, we let $\underline{\underline{P}} : (\mathbb{R}^d)^N \rightarrow \mathbb{X} \subset (\mathbb{R}^d)^N$ be the Euclidean space equivalent of \mathcal{P} , and similarly for the Euclidean equivalent $Q : \mathbb{R}^K \rightarrow \mathbb{W} \subset (\mathbb{R}^d)^K$ of \mathcal{Q} .

To simplify the next part of the presentation, we first consider the three-phase case in two space dimensions, whose setting is shown in Figure 1, i.e. $d = 2$, $I_S = I_R = 3$, $I_T = 2$. In addition, we assume that $\partial\Omega_D = \emptyset$. Then the solution to (4.3) can be written as $(Q\mathbf{W}^{m+1}, \kappa_\gamma^{m+1}, \vec{X}^m + \underline{\underline{P}}\delta\vec{X}^{m+1})$ for any solution of the linear system

$$\begin{pmatrix} QA_\Omega Q & O & Q\vec{N}_{\Omega,\Gamma}^\top \underline{\underline{P}} \\ B_{\Omega,\Gamma} Q & C_\Gamma & -\vec{D}_\Gamma^{(\beta)} \underline{\underline{P}} \\ O & \underline{\underline{P}}\vec{D}_\Gamma & \underline{\underline{P}}\underline{\underline{E}}_\Gamma^{(\gamma)} \underline{\underline{P}} \end{pmatrix} \begin{pmatrix} \mathbf{W}^{m+1} \\ \kappa_\gamma^{m+1} \\ \delta \vec{X}^{m+1} \end{pmatrix} = \begin{pmatrix} O \\ O \\ -\underline{\underline{P}}\underline{\underline{E}}_\Gamma^{(\gamma)} \underline{\underline{P}} \vec{X}^m \end{pmatrix}, \quad (5.1)$$

where $A_\Omega \in \mathbb{R}^{K \times K}$, $\vec{N}_{\Omega,\Gamma} \in (\mathbb{R}^d)^{N \times K}$, $B_{\Omega,\Gamma} \in \mathbb{R}^{N \times K}$, $C_\Gamma \in \mathbb{R}^{N \times N}$, $\vec{D}_\Gamma \in (\mathbb{R}^d)^{N \times N}$, $\vec{D}_\Gamma^{(\beta)} \in (\mathbb{R}^d)^{N \times N}$,

and $\underline{\underline{E}}_\Gamma^{(\gamma)} \in (\mathbb{R}^{d \times d})^{N \times N}$ are defined by

$$\begin{aligned} A_\Omega &:= \begin{pmatrix} A & O & O \\ O & A & O \\ O & O & A \end{pmatrix}, \quad \vec{N}_{\Omega, \Gamma} := \begin{pmatrix} O & \vec{N}_1 & -\vec{N}_1 \\ -\vec{N}_2 & O & \vec{N}_2 \\ \vec{N}_3 & -\vec{N}_3 & O \end{pmatrix}, \quad B_{\Omega, \Gamma} := \begin{pmatrix} O & B_1 & -B_1 \\ -B_2 & O & B_2 \\ B_3 & -B_3 & O \end{pmatrix}, \\ C_\Gamma &:= \begin{pmatrix} C_1 & O & O \\ O & C_2 & O \\ O & O & C_3 \end{pmatrix}, \quad \vec{D}_\Gamma := \begin{pmatrix} \vec{D}_1 & O & O \\ O & \vec{D}_2 & O \\ O & O & \vec{D}_3 \end{pmatrix}, \\ \vec{D}_\Gamma^{(\beta)} &:= \begin{pmatrix} \vec{D}_1^{(\beta)} & O & O \\ O & \vec{D}_2^{(\beta)} & O \\ O & O & \vec{D}_3^{(\beta)} \end{pmatrix}, \quad \underline{\underline{E}}_\Gamma^{(\gamma)} := \begin{pmatrix} \underline{\underline{E}}_1^{(\gamma)} & O & O \\ O & \underline{\underline{E}}_2^{(\gamma)} & O \\ O & O & \underline{\underline{E}}_3^{(\gamma)} \end{pmatrix}, \end{aligned}$$

with

$$\begin{aligned} [A]_{i,j} &:= \langle \nabla \Psi_j^m, \nabla \Psi_i^m \rangle_\Omega, & [\vec{N}_c]_{l,i} &:= \frac{1}{\tau_m} \langle \Phi_{c,l}^m, \Psi_i^m \rangle_{\Gamma_c^m}^{(h)} \vec{\omega}_{c,l}^m, \\ [B_c]_{k,j} &:= \langle \Psi_j^m, \Phi_{c,k}^m \rangle_{\Gamma_c^m}^{(h)}, & [C_c]_{k,l} &:= \langle \Phi_{c,l}^m, \Phi_{c,k}^m \rangle_{\Gamma_c^m}^h, \\ [\vec{D}_c]_{k,l} &:= \langle \Phi_{c,l}^m, \Phi_{c,k}^m \rangle_{\Gamma_c^m}^{\vec{h}} \vec{\omega}_{c,l}^m, & [\vec{D}_c^{(\beta)}]_{k,l} &:= \frac{1}{\tau_m} \langle \frac{\rho_c}{\beta_c(\vec{\nu}_c^m)} \Phi_{c,l}^m, \Phi_{c,k}^m \rangle_{\Gamma_c^m}^h \vec{\omega}_{c,l}^m, \\ [\underline{\underline{E}}_c^{(\gamma)}]_{k,l} &:= \left(\langle \nabla_s^{\vec{G}}(\Phi_{c,l}^m \vec{e}_j), \nabla_s^{\vec{G}}(\Phi_{c,k}^m \vec{e}_i) \rangle_{\gamma, \Gamma_c^m} \right)_{i,j=1}^d, \end{aligned}$$

for each $c \in \mathbb{N}_{\leq I_S}$, where $\{\vec{e}_j\}_{j \in \mathbb{N}_{\leq d}}$ denotes the Euclidean standard basis in \mathbb{R}^d .

The advantage of the system (5.1) over a naive implementation of (4.3) is that complications due to nonstandard finite element spaces are completely avoided. A disadvantage is, however, that the system (5.1) is highly singular, in that due to the presence of the projections the dimension of its kernel is larger than the dimension of the scalar bulk finite element space S^m . This makes it difficult to solve (5.1) in practice. A more practical formulation can be obtained by eliminating one of the components of \mathbf{W}^{m+1} . In particular, on recalling that $\mathbf{W}^{m+1} \cdot \mathbf{1} = 0$, we can reduce the unknown variables $\mathbf{W}^{m+1} \in \mathbb{R}^K$ to $(W_1^{m+1}, W_2^{m+1}) \in \mathbb{R}^{K-K_\Omega^m}$ by introducing the linear map $\hat{Q} : \mathbb{R}^{K-K_\Omega^m} \rightarrow \mathbb{W} \subset \mathbb{R}^K$ defined by

$$\hat{Q} := \begin{pmatrix} I_{K_\Omega^m} & O \\ O & I_{K-K_\Omega^m} \\ -I_{K_\Omega^m} & -I_{K-K_\Omega^m} \end{pmatrix},$$

where I_M denotes the identity matrix of size M for $M \in \mathbb{N}$. Then the solution to (4.3) can be written as $(\hat{Q} \hat{\mathbf{W}}^{m+1}, \kappa_\gamma^{m+1}, \vec{X}^m + \underline{\underline{P}} \delta \vec{X}^{m+1})$ for any solution of the reduced linear system

$$\begin{pmatrix} \hat{A}_\Omega & O & \hat{N}_{\Omega, \Gamma}^\top \underline{\underline{P}} \\ \hat{B}_{\Omega, \Gamma} & C_\Gamma & -\vec{D}_\Gamma^{(\beta)} \underline{\underline{P}} \\ O & \underline{\underline{P}} \vec{D}_\Gamma & \underline{\underline{P}} \underline{\underline{E}}_\Gamma^{(\gamma)} \underline{\underline{P}} \end{pmatrix} \begin{pmatrix} \hat{\mathbf{W}}^{m+1} \\ \kappa_\gamma^{m+1} \\ \delta \vec{X}^{m+1} \end{pmatrix} = \begin{pmatrix} O \\ O \\ -\underline{\underline{P}} \underline{\underline{E}}_\Gamma^{(\gamma)} \underline{\underline{P}} \vec{X}^m \end{pmatrix}, \quad (5.2)$$

where

$$\hat{A}_\Omega = \begin{pmatrix} A & O \\ O & A \end{pmatrix}, \quad \hat{B}_{\Omega, \Gamma} := B_{\Omega, \Gamma} \hat{Q} = \begin{pmatrix} B_1 & 2B_1 \\ -2B_2 & -B_2 \\ B_3 & -B_3 \end{pmatrix}, \quad \hat{N}_{\Omega, \Gamma} := \begin{pmatrix} O & \vec{N}_1 \\ -\vec{N}_2 & O \\ \vec{N}_3 & -\vec{N}_3 \end{pmatrix}.$$

In contrast to (5.1), the kernel of (5.2) is small, as it only involves the projections concerning the triple junction attachment conditions. Hence, iterative solution methods, combined with good preconditioners, work very well to solve (5.2) in practice.

Remark 5.1. *For illustrative purposes, we presented the matrix formulations (5.1) and (5.2) for the simple curve network shown in Figure 1, and for $\partial\Omega_D = \emptyset$. Extending these matrix formulations to general surface clusters and situations with $\partial\Omega_D \neq \emptyset$ is straightforward. For example, we obtain for the block matrices in (5.1) that $A_\Omega := \text{diag}(A)_{\ell=1,\dots,I_R}$, $\vec{N}_{\Omega,\Gamma} := ([\chi_\ell]_{\Gamma_c} \vec{N}_c)_{c=1,\dots,I_S,\ell=1,\dots,I_R}$, $B_{\Omega,\Gamma} := ([\chi_\ell]_{\Gamma_c} B_c)_{c=1,\dots,I_S,\ell=1,\dots,I_R}$, $C_\Gamma := \text{diag}(C_i)_{i=1,\dots,I_S}$, $\vec{D}_\Gamma := \text{diag}(\vec{D}_i)_{i=1,\dots,I_S}$, $\vec{D}_\Gamma^{(\beta)} := \text{diag}(\vec{D}_i^{(\beta)})_{i=1,\dots,I_S}$ and $\underline{\underline{E}}_\Gamma^{(\gamma)} := \text{diag}(\underline{\underline{E}}_i^{(\gamma)})_{i=1,\dots,I_S}$. Once again, the generalized system corresponding to (5.1) can be reduced by eliminating the final component $W_{I_R}^{m+1}$ from \mathbf{W}^{m+1} . We obtain the same block structure as in (5.2), with the new entries now given by $\hat{A}_\Omega = \text{diag}(A)_{\ell=1,\dots,I_R-1}$, $\hat{B}_{\Omega,\Gamma} = (([\chi_\ell]_{\Gamma_i} - [\chi_{I_R-1}]_{\Gamma_i})B_i)_{i=1,\dots,I_S,\ell=1,\dots,I_R-1}$ and $\hat{N}_{\Omega,\Gamma} = (-[\chi_\ell]_{\Gamma_i} \vec{N}_i)_{i=1,\dots,I_S,\ell=1,\dots,I_R-1}$.*

6 Numerical results

We implemented the fully discrete finite element approximation (4.3) within the finite element toolbox ALBERTA, see [33]. The arising linear systems of the form (5.2) are solved with a GMRes iterative solver with the following preconditioners. In 2D, we take as preconditioner a least squares solution of the block matrix in (5.2) without $\underline{\underline{P}}$. Due to the large memory requirements of this preconditioner in 3D, as an alternative in 3D we take as preconditioner a least squares solution of the lower triangular block of the matrix in (5.2) without $\underline{\underline{P}}$. For the computation of the least squares solution we employ the sparse factorization package SPQR, see [16], while for the inversion of nonsingular blocks we use the sparse factorization package UMFPACK, see [15].

We employ an unfitted finite element discretization. The precise description of the adaptively refined and coarsened bulk triangulations \mathcal{T}^m can be found in [7, §5.1], see also the recent works [18, 19, 23]. We stress that due to the unfitted nature of our finite element approximations, special quadrature rules need to be employed in order to assemble terms that feature both bulk and surface finite element functions. For all the computations presented in this section, we use true integration for these terms, and we refer to [7, 32] for details on the practical implementation. We note that our theoretical framework does not allow for changes of topology, e.g., the vanishing of an interface. Hence, following our previous work in [18], in our 2D computations we perform heuristic surgeries whenever a curve becomes too short. Here a closed curve is simply discarded, while a curve that was part of a network is removed. This will leave two triple junctions, where only two curves meet, and the involved curves can be glued together so that the simulation can continue. Throughout this section we use uniform time steps, in that $\tau_m = \tau$ for $m = 0, \dots, M-1$. Unless otherwise stated we choose $\rho_i = 1$ and $\beta_i \equiv 1$ for $i \in \mathbb{N}_{\leq I_S}$. We always choose $\Omega = (-4, 4)^d$.

In analogue to (2.11), we define the discrete energy as

$$\mathcal{E}^m = |\Gamma^m|_\gamma - \sum_{\ell=1}^{I_R} w_{D,\ell} \text{vol}(\mathcal{R}_\ell^m),$$

where \mathcal{R}_ℓ^m are the natural discrete analogues of the subdomains $\mathcal{R}_\ell[\Gamma(t_m)]$, $\ell = 1, \dots, I_R$. Moreover, we recall the convention that $w_D = \mathbf{0}$ when $\partial\Omega_N = \partial\Omega$.

In order to describe the orientations of the surface clusters with respect to the bulk regions they enclose, we follow the notation from [18] and define the matrices $\mathcal{O} \in \{-1, 0, 1\}^{I_R \times I_S}$ with entries

$$\mathcal{O}_{\ell i} = -[\chi_\ell]_{\Gamma_i}.$$

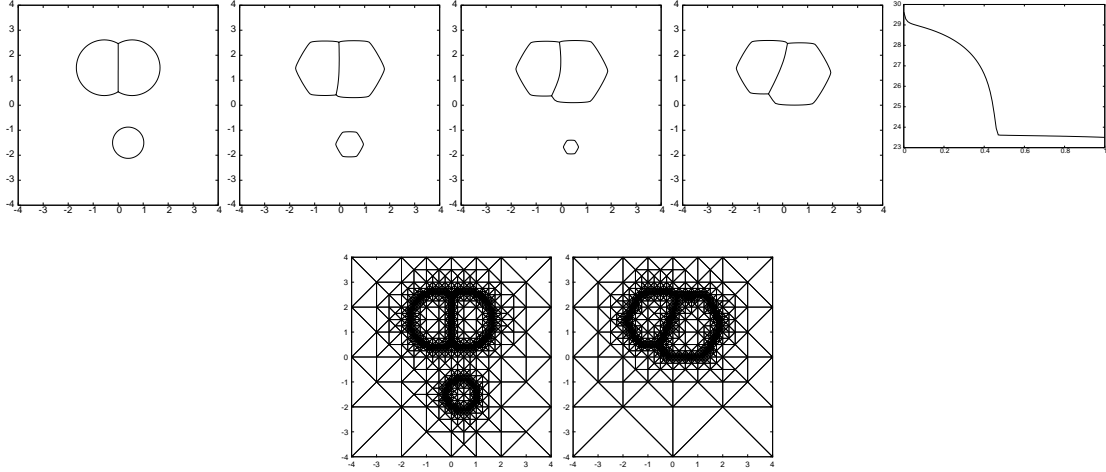


Figure 2: The solution at times $t = 0, 0.2, 0.4, 1$, and a plot of the discrete energy over time. Below we show the adaptive bulk mesh at times $t = 0$ and $t = 1$.

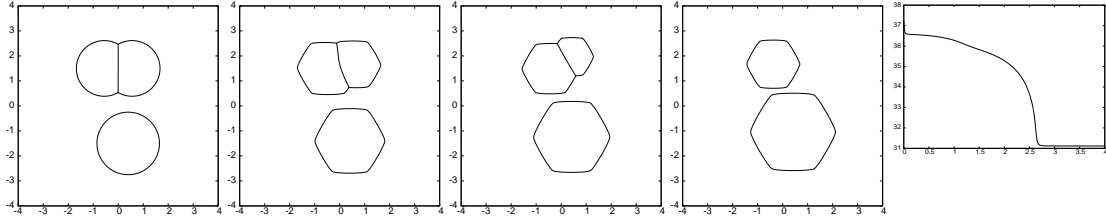


Figure 3: The solution at times $t = 0, 1, 2, 4$, and a plot of the discrete energy over time.

6.1 Simulations in 2D with $\partial\Omega_N = \partial\Omega$

In this subsection we consider some numerical simulations for $d = 2$ and $\partial\Omega_N = \partial\Omega$. We also let $\rho = 0$. For the anisotropy we define

$$\gamma_{\text{hex}}(\vec{p}) := \sum_{\ell=1}^3 \sqrt{[(R(\frac{\pi}{3})^\ell)^\top D(\delta)(R(\frac{\pi}{3}))^\ell \vec{p} \cdot \vec{p}], \quad \delta = 0.1, \quad (6.1)$$

where $R(\theta) = \begin{pmatrix} \cos \theta & \sin \theta \\ -\sin \theta & \cos \theta \end{pmatrix}$ and $D(\delta) = \text{diag}(1, \delta^2)$. Observe that the Wulff shape of (6.1) is given by a smoothed hexagon, see [4] for details. Unless otherwise stated, we choose $\gamma_i = \gamma_{\text{hex}}$, $i \in \mathbb{N}_{\leq I_S}$.

Example 1: We investigate how a standard double bubble and a disk evolve, when the first phase is made up of the left part of the double bubble, and the second phase is made up of the right part of the double bubble and the disk. We have $I_S = 4$, $I_R = 3$, $I_T = 2$, $(s_1^1, s_2^1, s_3^1) = (s_1^2, s_2^2, s_3^2) = (1, 2, 3)$ and $\mathcal{O} = \begin{pmatrix} 0 & -1 & 1 & 0 \\ 1 & 0 & -1 & -1 \\ -1 & 1 & 0 & 1 \end{pmatrix}$. The two bubbles of the double bubble enclose an area of about 3.139

each, while the disk has an initial radius of $\frac{5}{8}$, meaning it initially encloses an area of $\frac{25\pi}{64} \approx 1.227$. During the evolution the disk vanishes, and the right bubble grows correspondingly, see Figure 2. Repeating the simulation with a bigger initial disk gives the results in Figure 3. Here the radius is $\frac{5}{4}$, so that the enclosed area is 4.909. Now the disk grows at the expense of the right bubble, so that eventually two separate phases remain.

Example 2: We consider the evolution of two double bubbles. In particular, we have $I_S = 6$, $I_R = 3$,

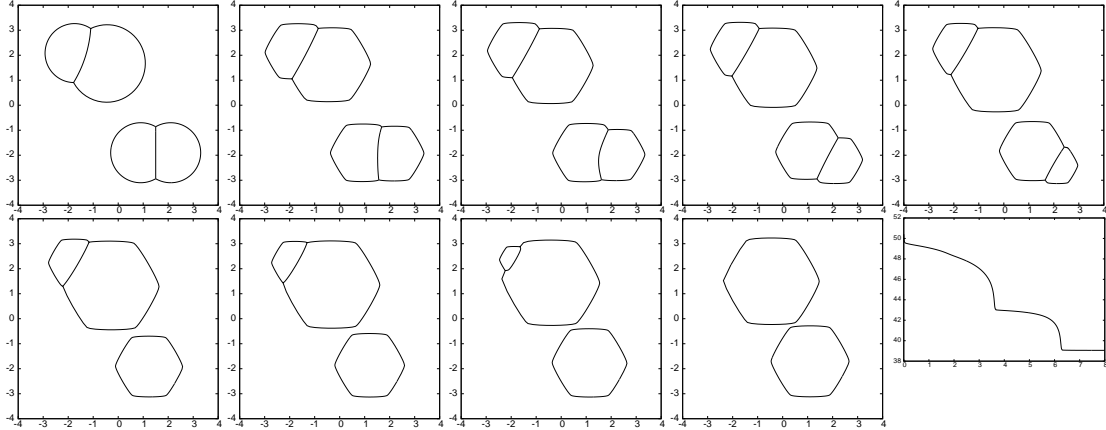


Figure 4: The solution at times $t = 0, 0.5, 1, 2, 3, 4, 5, 6, 7, 8$, and a plot of the discrete energy over time.

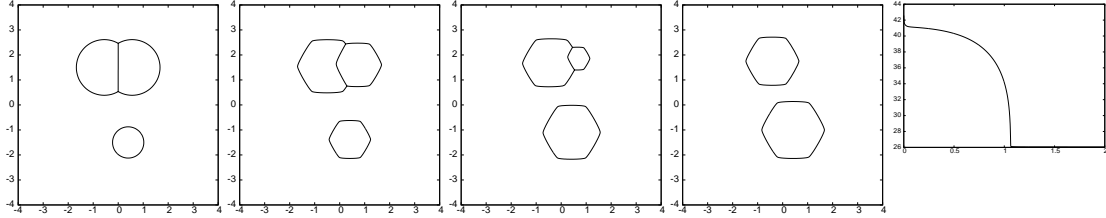


Figure 5: The solution at times $t = 0, 0.5, 1, 2$, and a plot of the discrete energy over time.

$I_T = 4$, $(s_1^1, s_2^1, s_3^1) = (s_1^2, s_2^2, s_3^2) = (1, 2, 3)$, $(s_1^3, s_2^3, s_3^3) = (s_1^4, s_2^4, s_3^4) = (4, 5, 6)$ and

$$\mathcal{O} = \begin{pmatrix} 0 & -1 & 1 & 0 & -1 & 1 \\ 1 & 0 & -1 & 1 & 0 & -1 \\ -1 & 1 & 0 & -1 & 1 & 0 \end{pmatrix}.$$

The first bubble is chosen with enclosing areas 3.14 and 6.48, while the second double bubbles encloses two areas of size 3.64. In each case, the left bubble is assigned to phase 1, while the right bubbles are assigned to phase 2. In this way, the lower double bubble holds the larger portion of phase 1, while the upper double bubble holds the larger portion of phase 2. Consequently, each double bubble evolves to a single disk that contains just one phase. See Figure 4.

Example 3: As an example for non-equal surface energy densities for the various curves, we repeat the simulation from Example 1 in Figure 2, but now choose $(\gamma_1, \gamma_2, \gamma_3, \gamma_4) = (2\gamma_{\text{hex}}, \gamma_{\text{hex}}, 2\gamma_{\text{hex}}, \gamma_{\text{hex}})$. That is, the curves 1 and 3 in the double bubble have twice the surface energy densities of the curves 2 and 4. This now means that in contrast to Figure 2, it makes energetically more sense to increase the size of the single bubble, while shrinking the bubble that is surrounded by the more expensive interfaces. See Figure 5 for the observed evolution.

6.2 Simulations in 2D with undercooling on $\partial\Omega$

In this subsection we consider some numerical simulations for $d = 2$ and $\partial\Omega_D \neq \emptyset$. For the anisotropy we define γ_{hex} as in (6.1) but now with $\delta = 0.01$. This leads to sharper corners in the Wulff shape.

Example 4: On the boundary $\partial\Omega = \partial\Omega_D$ we choose the undercooling parameters $\mathbf{w}_D = (20, 10, -30)^\top$, and start with a very small seed consisting of a standard double bubble. In fact, the two bubbles of the double bubble enclose an area of about 0.031 each. We also let $\rho = 1$. Moreover, we have $I_S = 3$,

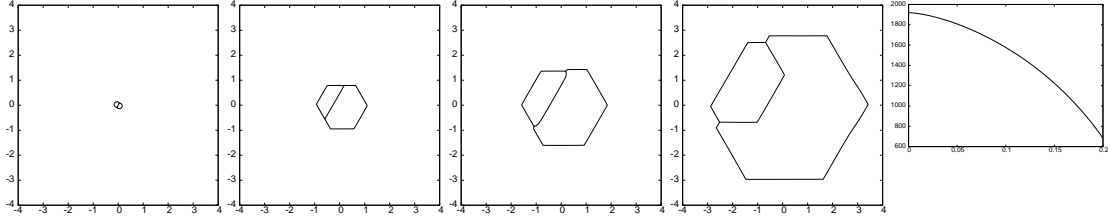


Figure 6: ($w_D = (20, 10, -30)^\top$, $\rho = 1$) The solution at times $t = 0, 0.05, 0.1, 0.2$, and a plot of the discrete energy over time.

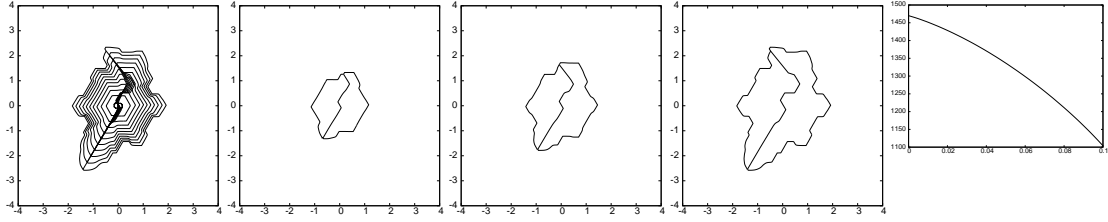


Figure 7: ($w_D = (12, 11, -23)^\top$, $\rho = \alpha = 0.05$) The solution at times $t = 0, 0.01, \dots, 0.1$, and separately at times $t = 0.05$, $t = 0.07$ and $t = 0.1$, and a plot of the discrete energy over time.

$I_R = 3$, $I_T = 2$, $(s_1^1, s_2^1, s_3^1) = (s_1^2, s_2^2, s_3^2) = (1, 2, 3)$ and $\mathcal{O} = \begin{pmatrix} 0 & -1 & 1 \\ 1 & 0 & -1 \\ -1 & 1 & 0 \end{pmatrix}$. The evolution is shown in Figure 6.

Example 5: In order to provoke some more unstable growths, we use the initial data from Example 4 and now set $w_D = (12, 11, -23)^\top$, $\rho = 0.05$, as well as $(\gamma_1, \gamma_2, \gamma_3) = \alpha(\gamma_{\text{hex}}, \gamma_{\text{hex}}, \gamma_{\text{hex}})$ where $\alpha = 0.05$. The evolution is shown in Figure 7. The same simulation but with the undercooling only applied to the right boundary is shown in Figure 8. That is, here $\partial\Omega_D = \{4\} \times (-4, 4)$, and we also move the initial seed further to the left to allow it more space to grown into. In fact, we can observe dendritic growth towards the undercooled part of the external boundary during the evolution.

Example 6: We use the initial data from Example 4 and now set $w_D = (5, 5 - 10)^\top$, $\rho = 0.05$, as well as $(\gamma_1, \gamma_2, \gamma_3) = \alpha(\gamma_{\text{hex}}, \gamma_{\text{hex}}, \gamma_{\text{hex}})$ where $\alpha = 0.005$. The simulation is shown in Figure 9, with the two crystals growing symmetrically. To break this symmetry, we next set $w_D = (10, 1, -11)^\top$, and let $\rho = 0.05$, as well as $(\gamma_1, \gamma_2, \gamma_3) = \alpha(\gamma_{\text{hex}}, \gamma_{\text{hex}}, \gamma_{\text{hex}})$ where $\alpha = 0.05$. The new evolution is far less symmetric, with the right crystal nearly enveloping the left one. See Figure 10. A further nonsymmetric example with $w_D = (1, 10, -11)^\top$, $\rho = 0.05$, as well as $(\gamma_1, \gamma_2, \gamma_3) = \alpha(\gamma_{\text{hex}}, \gamma_{\text{hex}}, \gamma_{\text{hex}})$ where $\alpha = 0.02$ is shown in Figure 11.

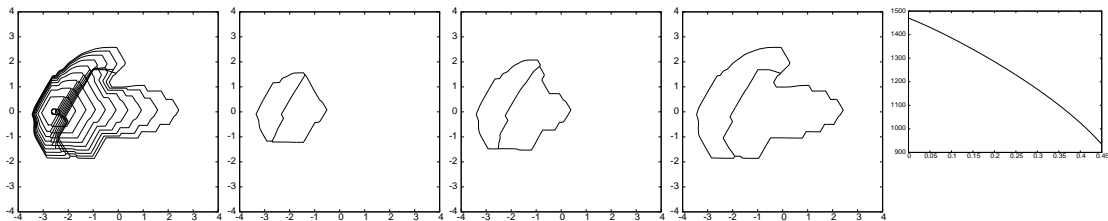


Figure 8: ($w_D = (12, 11, -23)^\top$, $\rho = \alpha = 0.05$) The solution at times $t = 0, 0.05, \dots, 0.45$, and separately at times $t = 0.2$, $t = 0.3$ and $t = 0.45$, and a plot of the discrete energy over time.

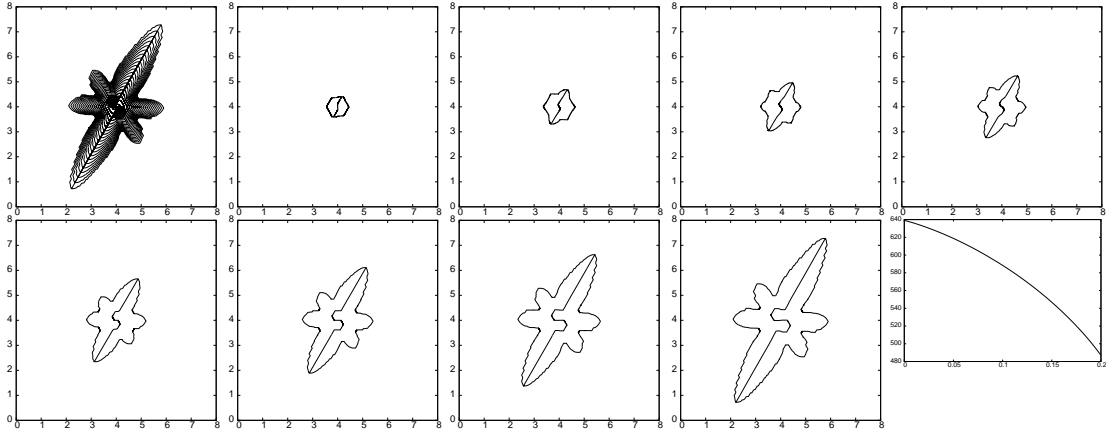


Figure 9: ($w_D = (5, 5, -10)^\top$, $\rho = 0.05$, $\alpha = 0.005$) The solution at times $t = 0, 0.01, \dots, 0.2$, and separately at times $t = 0.02, t = 0.04, t = 0.06, t = 0.08, t = 0.11, t = 0.14, t = 0.17$ and $t = 0.2$, and a plot of the discrete energy over time.

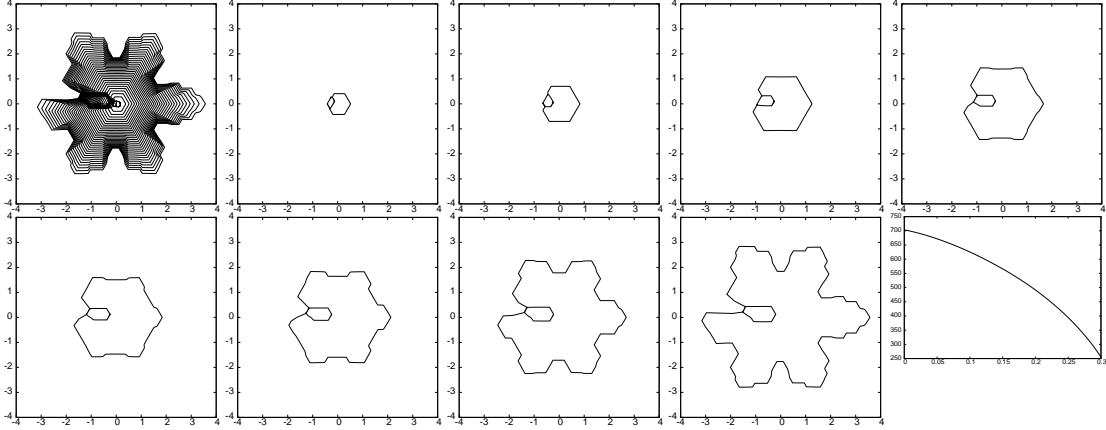


Figure 10: ($w_D = (10, 1, -11)^\top$, $\rho = \alpha = 0.05$) The solution at times $t = 0, 0.01, \dots, 0.3$, and separately at times $t = 0.02, t = 0.05, t = 0.1, t = 0.15, t = 0.17, t = 0.2, t = 0.25$ and $t = 0.3$, and a plot of the discrete energy over time.

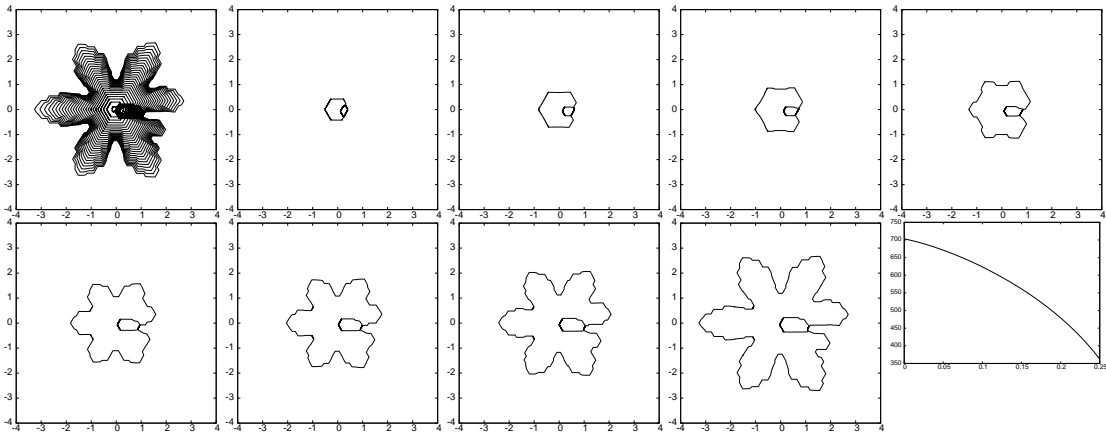


Figure 11: ($w_D = (1, 10, -11)^\top$, $\rho = 0.05$, $\alpha = 0.02$) The solution at times $t = 0, 0.01, \dots, 0.3$, and separately at times $t = 0.02, t = 0.05, t = 0.07, t = 0.1, t = 0.15, t = 0.17, t = 0.2$ and $t = 0.25$, and a plot of the discrete energy over time.

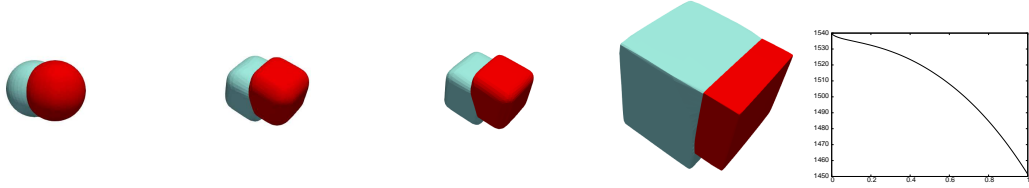


Figure 12: ($\mathbf{w}_D = (2, 1, -3)^\top$, $\rho = 1$) The solution at times $t = 0, 0.05, 0.1, 1$, and a plot of the discrete energy over time.

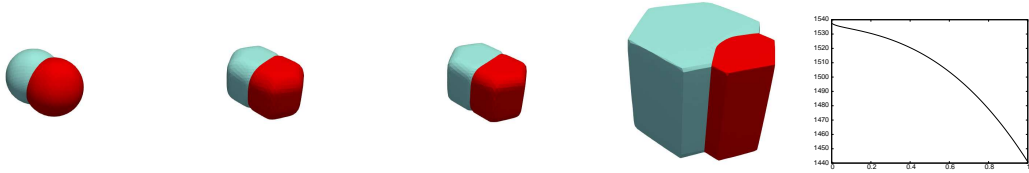


Figure 13: ($\mathbf{w}_D = (2, 1, -3)^\top$, $\rho = 1$) The solution at times $t = 0, 0.05, 0.1, 1$, and a plot of the discrete energy over time.

6.3 Numerical results in 3D

In this subsection we consider some numerical simulations for $d = 3$ and $\partial\Omega_D = \partial\Omega$. For the possible anisotropies we define first of all

$$\gamma_{\ell^1}(\vec{p}) = \sum_{i=1}^3 \sqrt{\delta^2 |\vec{p}|^2 + p_i^2 (1 - \delta^2)}, \quad \delta = 0.01, \quad (6.2)$$

which approximates the ℓ^1 -norm of \vec{p} , see [5]. In addition, a 3D analogue of (6.1), compare with [9, (13)], is defined by

$$\gamma_{\text{hex}}(\vec{p}) := l_\delta(R_2(\frac{\pi}{2})\vec{p}) + \frac{1}{\sqrt{3}} \sum_{\ell=1}^3 l_\delta(R_1(\theta_0 + \ell \frac{\pi}{3})\vec{p}), \quad \delta = 0.01, \quad (6.3)$$

where $R_1(\theta) := \begin{pmatrix} \cos \theta & \sin \theta & 0 \\ -\sin \theta & \cos \theta & 0 \\ 0 & 0 & 1 \end{pmatrix}$ and $R_2(\theta) := \begin{pmatrix} \cos \theta & 0 & \sin \theta \\ 0 & 1 & 0 \\ -\sin \theta & 0 & \cos \theta \end{pmatrix}$ are rotation matrices, and where

$l_\delta(\vec{p}) := [\delta^2 |\vec{p}|^2 + p_1^2 (1 - \delta^2)]^{\frac{1}{2}}$. The Wulff shape of the anisotropy (6.3) is given by a smoothed hexagonal prism, see e.g. [9, Fig. 3].

In order to be able to vary the kinetic coefficient β for the simulations in this subsection, we define

$$\beta_{\text{flat}}(\vec{p}) = \beta_{\text{flat}, \ell}(\vec{p}) := \sqrt{p_1^2 + p_2^2 + 10^{-2\ell} p_3^2} \quad (6.4)$$

with $\ell \in \mathbb{N}$. For the surface clusters we always choose a double bubble, so that $I_S = 3$, $I_R = 3$, $I_T = 1$,

$$(s_1^1, s_2^1, s_3^1) = (1, 2, 3) \text{ and } \mathcal{O} = \begin{pmatrix} 0 & -1 & 1 \\ 1 & 0 & -1 \\ -1 & 1 & 0 \end{pmatrix}.$$

Example 7: On the boundary $\partial\Omega = \partial\Omega_D$ we choose the undercooling parameters $\mathbf{w}_D = (2, 1, -3)^\top$, and start with a seed consisting of a standard double bubble. The two bubbles of the double bubble enclose a volume of about 2.1 each. We also let $\rho = 1$. For the anisotropies we choose $\gamma_i = \gamma_{\ell^1}$, $i \in \mathbb{N}_{\leq I_S}$, recall (6.2). The evolution is shown in Figure 12. When we choose $\gamma_i = \gamma_{\text{hex}}$, $i \in \mathbb{N}_{\leq I_S}$, recall (6.3), we obtain the evolution shown in Figure 13.

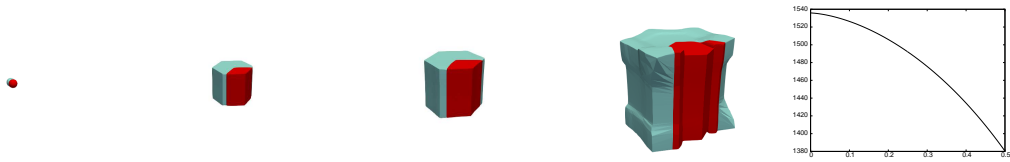


Figure 14: ($w_D = (2, 1, -3)^\top$, $\rho = \alpha = 0.05$) The solution at times $t = 0, 0.1, 0.2, 0.5$, and a plot of the discrete energy over time.

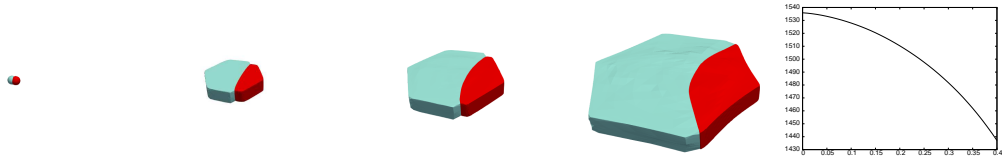


Figure 15: ($w_D = (2, 1, -3)^\top$, $\rho = \alpha = 0.05$, $\beta = \beta_{\text{flat},3}$) The solution at times $t = 0, 0.1, 0.2, 0.4$, and a plot of the discrete energy over time.

Example 8: We use the same setup as in Example 7, but now let $\rho = 0.05$. In addition, we choose $(\gamma_1, \gamma_2, \gamma_3) = \alpha(\gamma_{\text{hex}}, \gamma_{\text{hex}}, \gamma_{\text{hex}})$, $i \in \mathbb{N}_{\leq I_S}$, recall (6.3), with $\alpha = 0.05$. Moreover, we choose either $\beta_i \equiv 1$ or $\beta_i = \beta_{\text{flat},3}$, $i \in \mathbb{N}_{\leq I_S}$, recall (6.4). The evolutions are shown in Figures 14 and 15, respectively.

Example 9: We use a similar setup to Example 7, but now let $\rho = 0.05$ and set $w_D = (2, 0.2, -2.2)^\top$. We also start with a smaller seed. In fact, the two bubbles of the initial double bubble both enclose a volume of about 0.017. In addition, we choose $(\gamma_1, \gamma_2, \gamma_3) = \alpha(\gamma_{\text{hex}}, \gamma_{\text{hex}}, \gamma_{\text{hex}})$, $i \in \mathbb{N}_{\leq I_S}$, recall (6.3), with $\alpha = 0.05$. The evolution is shown in Figure 16.

References

- [1] W. BAO, H. GARCKE, R. NÜRNBERG, AND Q. ZHAO, *A structure-preserving finite element approximation of surface diffusion for curve networks and surface clusters*, Numer. Methods Partial Differ. Eq., 39 (2023), pp. 759–794.
- [2] J. W. BARRETT, J. F. BLOWEY, AND H. GARCKE, *On fully practical finite element approximations of degenerate Cahn–Hilliard systems*, M2AN Math. Model. Numer. Anal., 35 (2001), pp. 713–748.
- [3] J. W. BARRETT, H. GARCKE, AND R. NÜRNBERG, *On the variational approximation of combined second and fourth order geometric evolution equations*, SIAM J. Sci. Comput., 29 (2007), pp. 1006–1041.
- [4] ———, *Numerical approximation of anisotropic geometric evolution equations in the plane*, IMA J. Numer. Anal., 28 (2008), pp. 292–330.

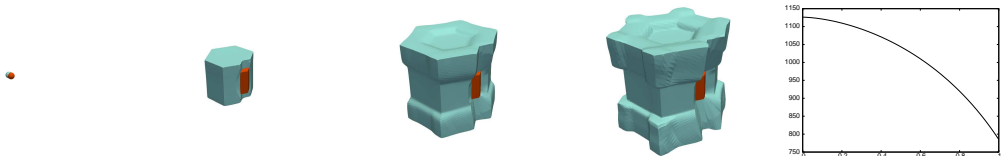


Figure 16: ($w_D = (2, 0.3, -2.2)^\top$, $\rho = \alpha = 0.05$) The solution at times $t = 0, 0.2, 0.8, 1$, and a plot of the discrete energy over time.

- [5] ———, *A variational formulation of anisotropic geometric evolution equations in higher dimensions*, Numer. Math., 109 (2008), pp. 1–44.
- [6] ———, *Finite element approximation of coupled surface and grain boundary motion with applications to thermal grooving and sintering*, European J. Appl. Math., 21 (2010), pp. 519–556.
- [7] ———, *On stable parametric finite element methods for the Stefan problem and the Mullins–Sekerka problem with applications to dendritic growth*, J. Comput. Phys., 229 (2010), pp. 6270–6299.
- [8] ———, *Parametric approximation of surface clusters driven by isotropic and anisotropic surface energies*, Interfaces Free Bound., 12 (2010), pp. 187–234.
- [9] ———, *Numerical computations of faceted pattern formation in snow crystal growth*, Phys. Rev. E, 86 (2012), p. 011604.
- [10] ———, *Parametric finite element approximations of curvature-driven interface evolutions*, in Geometric partial differential equations. Part I, vol. 21 of Handb. Numer. Anal., Elsevier/North-Holland, Amsterdam, 2020, pp. 275–423.
- [11] J. F. BLOWEY, M. I. M. COPETTI, AND C. M. ELLIOTT, *Numerical analysis of a model for phase separation of a multi-component alloy*, IMA J. Numer. Anal., 16 (1996), pp. 111–139.
- [12] L. BRONSARD, H. GARCKE, AND B. STOTH, *A multi-phase Mullins–Sekerka system: matched asymptotic expansions and an implicit time discretisation for the geometric evolution problem*, Proc. Roy. Soc. Edinburgh Sect. A, 128 (1998), pp. 481–506.
- [13] D. DANILOV AND B. NESTLER, *Phase-field simulations of solidification in binary and ternary systems using a finite element method*, J. Cryst. Growth, 275 (2005), pp. e177–e182.
- [14] S. H. DAVIS, *Theory of Solidification*, Cambridge Monographs on Mechanics, Cambridge University Press, Cambridge, 2001.
- [15] T. A. DAVIS, *Algorithm 832: UMFPACK V4.3—an unsymmetric-pattern multifrontal method*, ACM Trans. Math. Software, 30 (2004), pp. 196–199.
- [16] ———, *Algorithm 915, SuiteSparseQR: Multifrontal multithreaded rank-revealing sparse QR factorization*, ACM Trans. Math. Software, 38 (2011), pp. 1–22.
- [17] G. DEMANGE, H. ZAPOLSKY, R. PATTE, AND M. BRUNEL, *A phase field model for snow crystal growth in three dimensions*, Comput. Mater., 3 (2017), p. 15.
- [18] T. ETO, H. GARCKE, AND R. NÜRNBERG, *A structure-preserving finite element method for the multi-phase Mullins–Sekerka problem with triple junctions*, Numer. Math., 156 (2024), pp. 1479–1509.
- [19] ———, *A parametric finite element method for a degenerate multi-phase Stefan problem with triple junctions*, Comput. Methods Appl. Math., 26 (2026), pp. 43–67.
- [20] D. J. EYRE, *Systems of Cahn–Hilliard equations*, SIAM J. Appl. Math., 53 (1993), pp. 1686–1712.
- [21] H. GARCKE, B. NESTLER, AND B. STINNER, *A diffuse interface model for alloys with multiple components and phases*, SIAM J. Appl. Math., 64 (2004), pp. 775–799.
- [22] H. GARCKE, B. NESTLER, AND B. STOTH, *On anisotropic order parameter models for multi-phase systems and their sharp interface limits*, Phys. D, 115 (1998), pp. 87–108.
- [23] H. GARCKE, R. NÜRNBERG, AND Q. ZHAO, *A variational front-tracking method for multiphase flow with triple junctions*, Math. Comp., 95 (2026), pp. 647–682.
- [24] H. GARCKE AND T. STURZENHECKER, *The degenerate multi-phase Stefan problem with Gibbs–Thomson law*, Adv. Math. Sci. Appl., 8 (1998), pp. 929–941.
- [25] D. HERLACH, ed., *Phase Transformations in Multicomponent Melts*, John Wiley & Sons, Ltd, 2008.

- [26] D. W. HOFFMAN AND J. W. CAHN, *A vector thermodynamics for anisotropic surfaces: I. fundamentals and application to plane surface junctions*, *Surface Sci.*, (1972), pp. 368–388.
- [27] Y. LI AND W. BAO, *An energy-stable parametric finite element method for anisotropic surface diffusion*, *J. Comput. Phys.*, 446 (2021), p. 110658.
- [28] Y. LI, J. CHOI, AND J. KIM, *Multi-component Cahn–Hilliard system with different boundary conditions in complex domains*, *J. Comput. Phys.*, 323 (2016), pp. 1–16.
- [29] K. G. LIBBRECHT, *The physics of snow crystals*, *Rep. Progr. Phys.*, 68 (2005), pp. 855–895.
- [30] B. NESTLER, H. GARCKE, AND B. STINNER, *Multicomponent alloy solidification: Phase-field modeling and simulations*, *Phys. Rev. E*, 71 (2005), p. 041609.
- [31] R. NÜRNBERG, *Numerical simulations of immiscible fluid clusters*, *Appl. Numer. Math.*, 59 (2009), pp. 1612–1628.
- [32] ———, *A structure preserving front tracking finite element method for the Mullins–Sekerka problem*, *J. Numer. Math.*, 31 (2023), pp. 137–155.
- [33] A. SCHMIDT AND K. G. SIEBERT, *Design of Adaptive Finite Element Software: The Finite Element Toolbox ALBERTA*, vol. 42 of *Lecture Notes in Computational Science and Engineering*, Springer-Verlag, Berlin, 2005.
- [34] I. STEINBACH, *Phase-field models in materials science*, *Modelling and Simulation in Materials Science and Engineering*, 17 (2009), p. 073001.